G3 Genes | Genomes | Genetics

MUTANT SCREEN REPORT

A Forward Genetic Approach to Mapping a *P*-Element Second Site Mutation Identifies *DCP2* as a Novel Tumor Suppressor in *Drosophila melanogaster*

Rakesh Mishra,*,[1] Rohit Kunar,*,[1] Lolitika Mandal,[†] Debasmita Pankaj Alone,[‡] Shanti Chandrasekharan,[§] Anand Krishna Tiwari, Madhu Gwaldas Tapadia,* Ashim Mukherjee,[††] and Jagat Kumar Roy*,[2]**

*Cytogenetics Laboratory, Department of Zoology, Institute of Science, Banaras Hindu University, Varanasi 221005, India, [†]Department of Biological Sciences, Indian Institute of Science Education and Research Mohali, Manauli 140306, India, [‡]School of Biological Sciences, National Institute of Science Education and Research, HBNI, Jatni, Khurda 752050, India, [§]Division of Genetics, Indian Agricultural Research Institute, Pusa, New Delhi 110012, India, **School of Biological Sciences and Biotechnology, Indian Institute of Advanced Research, Koba, Gandhinagar-382 007, India, and [††]Department of Molecular and Human Genetics, Institute of Science, Banaras Hindu University, Varanasi 221005, India

ORCID IDs: 0000-0001-7352-8293 (R.M.); 0000-0003-1606-4992 (R.K.); 0000-0002-7711-6090 (L.M.); 0000-0003-4809-925X (D.P.A.); 0000-0002-4080-6653 (A.K.T.); 0000-0002-5050-4624 (M.G.T.); 0000-0002-3523-7089 (A.M.); 0000-0002-6461-3274 (J.K.R.)

ABSTRACT The use of transposons to create mutations has been the cornerstone of *Drosophila* genetics in the past few decades. Second-site mutations caused by transpositions are often devoid of transposons and thereby affect subsequent analyses. In a *P*-element mutagenesis screen, a second site mutation was identified on chromosome 3, wherein the homozygous mutants exhibit classic hallmarks of tumor suppressor mutants, including brain tumor and lethality; hence the mutant line was initially named as *lethal (3) tumorous brain* [*l(3)tb*]. Classical genetic approaches relying on meiotic recombination and subsequent complementation with chromosomal deletions and gene mutations mapped the mutation to CG6169, the mRNA decapping protein 2 (*DCP2*), on the left arm of the third chromosome (3L). Thus the mutation was renamed as $DCP2^{l(3)tb}$. Fine mapping of the mutation further identified the presence of a *Gypsy*-LTR like sequence in the 5′UTR coding region of *DCP2*, along with the expansion of the adjacent upstream intergenic AT-rich sequence. The mutant phenotypes are rescued by the introduction of a functional copy of *DCP2* in the mutant background, thereby establishing the causal role of the mutation and providing a genetic validation of the allelism. With the increasing repertoire of genes being associated with tumor biology, this is the first instance of mRNA decapping protein being implicated in *Drosophila* tumorigenesis. Our findings, therefore, imply a plausible role for the mRNA degradation pathway in tumorigenesis and identify *DCP2* as a potential candidate for future explorations of cell cycle regulatory mechanisms.

KEYWORDS
DCP2
tumor suppressor
Drosophila
genetic mapping
forward genetics

With increasing interest in studies of classical tumor suppressors (Papagiannouli and Mechler 2013; Ivanov *et al.*, 2010), the search for new candidate proteins in tumor suppression has garnered much importance (Tipping and Perrimon 2014). In *Drosophila*, *P*-element mutagenesis provides a convenient method to identify, isolate and clone tagged genes (Mechler 1994). Although identification and subsequent molecular analysis is convenient with *P*-element transpositions, second–site mutations devoid of any *P*-element insertion created during transposition, may impede further analyses (Liebl *et al.*, 2006). A *P*-element, *P-lac* w^+ (Bier *et al.*, 1989), on third chromosome at 93B position was mobilized via enhancer-trap mutagenesis to obtain regulators of *hsrω* at 93D3-4 region (Lakhotia and Tapadia 1998). In the process, one mutant line showed prolonged larval life, brain tumor in the larval brain and lethality in the late larval and pupal stages in homozygous condition. The escapee flies showed ommatidial defects and reduced survival. Molecular mapping approaches identified the *P*-element (*P-lac* w^+) to reside 94 bases downstream to the TATA box of *Rab11* (located at the cytogenetic position 93B12-13), which is 45 bases upstream to the first exon of the gene and is a part of the 5′UTR (Mandal and Roy, unpublished). *Rab11* codes for a vesicular trafficking protein and is a component of the recycling endosomes (Novick and Zerial 1997; Satoh *et al.*, 1997).

Introduction of a functional copy of *Rab11* in the homozygous mutant background rescued the ommatidial defect, but failed to rescue the tumorous phenotype and lethality, implying the presence of a second-site mutation, besides the *P*-element insertion in *Rab11*. Allowing free recombination, the mutations, *viz*., the *P*-element insertion in *Rab11* and the second-site mutation devoid of the *P*-element, were separated into two discrete isogenised lines (Alone and Roy, unpublished). Since the phenotypes shown by the second-site mutation phenocopies mutations in tumor suppressor genes in *Drosophila* (Gateff and Schneiderman 1969; Gateff 1994; Gateff E, 1978), the mutation was named as *l(3)tb* [*lethal (3) tumorous brain*] owing to its location on the third chromosome and the phenotypes manifested. Genetic and molecular analyses mapped the mutation to *DCP2* on the left arm of chromosome 3 (cytogenetic position 72A1) and hence the allele was named as $DCP2^{l(3)tb}$.

DCP2 codes for the mRNA decapping protein 2, which belongs to the NUDIX family of pyrophosphatases and was identified more than a decade ago through a yeast genetic screen (Dunckley and Parker 1999). Being one of the major components of the decapping complex, DCP2 is conserved in worms, flies, plants, mice, and humans (Wang *et al.*, 2002). DCP2 is activated by DCP1 and they function together as a holoenzyme to cleave the 5′ cap structure of mRNA (LaGrandeur and Parker 1998; Coller and Parker 2004; Parker and Song 2004; She *et al.*, 2008).

In humans, DCP2 is upregulated in lung cancer (Watson *et al.*, 2008) and regulates histone mRNA titres (Mullen and Marzluff 2008) and there is some evidence that DCP2 is regulated by the p53-DREAM pathway (Engeland 2018). Recently, Gaviraghi and coworkers showed that the co-activator of mRNA decapping, PNRC1, shuffles the mRNA decapping complex to the nucleolus from the P-bodies, wherein decapping of certain snoRNAs involved in processing of ribosomal RNA is initiated, thereby restricting the oncogenic potential of cells (Gaviraghi *et al.*, 2018; Mugridge and Gross 2018).

In *Drosophila*, *DCP2* plays fundamental roles in the response pathways active following chronic nicotine exposure and its loss mediates locomotor hyperactivity following such exposure (Ren *et al.*, 2012). Also, DCP2 is involved in the decapping of mRNAs involved in cell cycle progression and DNA replication and acts to restrict bunyaviral infections in cell lines and adult flies (Hopkins *et al.*, 2013).

Despite the abundance of information from various model organisms pertaining to the roles of the mRNA decapping machinery, and/or the decay programs in cellular homeostasis, development and stress management, our understanding of the roles of the components of the mRNA decay program(s) and their interaction with the cellular signaling modules *vis-à-vis* gene expression programs is still in its infancy. Although mRNA decapping plays a significant role in mRNA turnover and translation, widely affecting gene expression (Mitchell and Tollervey 2001; Raghavan and Bohjanen 2004; Song *et al.*, 2010), simultaneous links between mRNA degradation genes, retrotransposons and tumors have not been observed and/or investigated so far. Therefore, the novel allele $DCP2^{l(3)tb}$ reveals a new perception for functional roles of mutant lesions and the ensuing perturbations in gene regulation in tumor biology.

doi: https://doi.org/10.1534/g3.120.401501
Manuscript received May 25, 2020; accepted for publication June 23, 2020; published Early Online June 26, 2020.

Supplemental material available at figshare: https://doi.org/10.25387/g3.12568265.
[1]These authors contributed equally to the work.
[2]Corresponding author: Cytogenetics Laboratory, Department of Zoology, Institute of Science, Banaras Hindu University, Varanasi–221005, India. E-mail: jkroy@bhu.ac.in

MATERIALS AND METHODS

Fly strains and rearing conditions

All flies were raised on standard agar-cornmeal medium at 24 ± 1°. *Oregon* R^+ was used as the wild type control. The *l(3)tb* mutation (*y w*; +/+; *l(3)tb* /*TM6B*, Tb^1, *Hu*, e^1) was isolated in a genetic screen and the mutation was maintained with the *TM6B* balancer. The multiply marked "*rucuca*" (*ru h th st cu sr e ca/TM6B*, *Tb*) and "*ruPrica*" (*ru h th st cu sr e Pr ca/TM6B*, *Tb*) chromosomes were employed for recombination mapping (Lindsley and Zimm 1992). *w*; Δ*2-3*, *Sb/TM6B*, Tb^1, *Hu*, e^1 (Cooley *et al.* 1988) and *CyO*, *P{Tub-Pbac/T}2/*$Wg^{Sp\text{-}1}$;+/*TM6B*, *Tb*, *Hu*, e^1 were used for providing transposase source for *P* element and *piggyBac* specific transposable element, respectively, in mutagenesis experiment. The y^1w; *P{Act5C-GAL4}25F01/CyO*, *y w*; +/+; *Tub-GAL4/ TM3*, *Sb*, *e*, and *Elav-GAL4* stocks were obtained from the Bloomington *Drosophila* Stock Center. The lethal insertion mutants of gene *DCP2*, *viz*., *PBac{RB}*$DCP2^{e00034}$/*TM6B*, Tb^1 *Hu*, e^1 (Thibault *et al.* 2004) and *P{GT1}*$DCP2^{BG01766}$/*TM3*, Sb^1, e^1 (Lukacsovich *et al.* 2001) were obtained from Exelixis Stock Center, Harvard University and Bloomington *Drosophila* stock center, respectively, while the *UAS-*dbo^{RNAi} line used for knock-down of *diablo* (*dbo*) was procured from the Bloomington *Drosophila* Stock Center.

Deficiency stock *Df(3L)RM96* was generated in the laboratory (for details of characterization, refer to Supplementary Table S3) using progenitor *P* element stocks, *viz*, *P{RS5}5-SZ-3486*, *P{RS5}5-SZ-3070*, *P{RS3}UM-8356-3*, *P{RS3}UM-8241-3*, *P{RS3}CB-0072-3*, *y w P{70FLP*, ry^+*}3*F^{iso}/y^+Y; 2^{iso}; *TM2/TM6C*, *Sb*, w^{1118}_{iso}/y^+Y; 2^{iso}; *TM2/TM6C*, *Sb* obtained from Vienna *Drosophila* Resource Center (Golic and Golic 1996; Ryder *et al.* 2007). Various deficiency stocks and transposon insertion fly stocks (Supplementary Tables S1 and S2) used for complementation analysis were obtained from Bloomington *Drosophila* stock center and Exelixis stock center.

Analysis of lethal phase in l(3)tb homozygotes

For analysis of lethal phase and morphological anomalies associated with the homozygous *l(3)tb* mutation, embryos were collected at the intervals of 2h on food filled Petri dishes. Embryos from wild type flies were collected as controls. The total number of eggs in each plate was counted and the embryos were allowed to grow at 23° or 18° or 16° (±1°). Hatching of embryos and further development of larval stages was monitored to determine any developmental delay. Mutant larvae, at different stages, were dissected and the morphology of larval structures was examined.

Identification of mutant locus

Meiotic recombination mapping of l(3)tb mutation: Genetic recombination with multiple recessive chromosome markers, *ru cu ca*, was performed to map mutation in *y w*: +/+; *l(3)tb/TM6B, Tb* mutant. The *y w; l(3)tb/TM6B* males were crossed to virgin +/+; *ru Pri ca/TM6B* females to recover *l(3)tb* without *y w* on X-chromosome. The F1 *l(3)tb/TM6B* males were crossed to virgin +/+; *ru cu ca* females and the F2 progeny +/+; *l(3)tb/ru cu ca* virgin females were selected. These

F2 virgins were then crossed to *ru Pri ca/TM6B* males to score the frequency of recombinants in the F3 progeny. Thereafter, all the F3 progeny males obtained, were individually scored for *ru, h, th, st, cu, sr, e* and *ca* phenotypes and then they were individually crossed with virgin *l(3)tb/TM6B* females to identify which of them had the *l(3)tb* mutation along with other scored markers.

Complementation mapping of the l(3)tb mutation: Complementation analysis of the mutation in *l(3)tb* allele was carried out in two stages. First, deficiency stocks spanning the entire chromosome 3 (Supplementary Table S1) were used to identify the mutant loci, and second, lethal *P*-insertion alleles selected from the region narrowed down through recombination and deficiency mapping (Supplementary Table S2) were harnessed to further identify the mutant gene(s) in *l(3)tb*. In either case, virgin females of *y w*; +/+; *l(3)tb/TM6B,Tb* were crossed with the males of the various deficiency stocks and/or the lethal *P*-insertion alleles and the non-tubby F1 males heterozygous for *l(3)tb* and the deficiency were scored for the phenotype(s).

Reversion analysis was performed by the excision of *piggyBac* transposon in $DCP2^{e00034}$ with the help of *piggyBac* specific transposase source, *CyO, P{Tub-Pbac}2/wg*$^{SP-1}$ (Thibault *et al.* 2004) or by the excision of *P*-element in $DCP2^{BG01766}$ strain using transposase from the 'jumpstarter', *Δ2-3,Sb/TM6B, Tb*^{1}, *Hu, e*^{1}. Virgin flies from the 'mutator stocks', *viz.*, $DCP2^{e00034}$ or $DCP2^{BG01766}$ strain were crossed to male flies from respective 'jumpstarter stock'. F1 male flies with mosaic eye pigmentation carrying both the transposase and respective transposons were selected and crossed to JSK-3 (*TM3, Sb, e*^{1}*/TM6B, Tb*^{1}, *Hu, e*^{1}) virgins and from the next generation (F2), rare white eyed revertant flies were selected (Figure S1).

Fine mapping of l(3)tb mutation

Genomic DNA Isolation, PCR and Southern hybridization: Genomic DNA for polymerase chain reaction (PCR) was isolated by homogenizing 50 male flies from each of the desired genotype or 80-100 third instar larvae from homozygous mutant *l(3)tb* (Sambrook *et al.* 1989). Based on the results obtained from genetic mapping, identification of the candidate region in *DCP2* was done by overlapping PCR based screening, wherein the entire genomic span of *DCP2* was amplified using 28 primer pairs from 3L:15811834..15819523 (Supplementary Tables S4, S5, S6). After identifying the candidate region, it was validated with the primer pair, Dbo_F: 5′-ACAACATTCACTCCATGGAACACCT-3′ and DCP2_P19_R: 5′-TGCTCACCGAACTTTTTCGCGATCT-3′. The primer pair DCP2_F: 5′-ATAACAAAAAAGTTATGGTACCACCCCCGCGTTGTATTCT-3′ and DCP2_R: 5′-AGATTTCGATGTATATGGATCCGTCCCAACCTTTGCGTCT-3′ was designed to amplify the full length gene along with flanking sequences (500 bp on either side). In either case, the thermal cycling parameters included an initial denaturation at 96° (2 min) followed by 30 cycles of 30 s at 94°, 45 s at 72°, and 15 min at 68°. Final extension was carried out at 68° for 20 min. The PCR products were electrophoresed on 0.8% agarose gel with O'GeneRuler 1 kb plus DNA ladder (Thermo Scientific, USA). An 812 bp region (3L: 15825979..15826790) spanning the candidate mutated region in *DCP2* was PCR amplified and ligated in pGEM-T vector (Promega) to generate the pGEM-T-812 clone. The ~430 bp fragment isolated during primer walking (see below) was purified and ligated in pTopo-TA-XL vector (Invitrogen, USA) to generate the pTopo-TA-XL-430 clone. Digestion, ligation and transformation were performed using standard protocols as described in Sambrook *et al.* 1989. Southern hybridizations were performed according to Russell and Sambrook 2001. Following electrophoresis and gel pre-treatments, DNA was transferred on to positively charged nylon membranes (Roche, Germany). Hybridizations were performed at 68° with 0.02% SDS, 5X SSC, 0.5% Blocking reagent, and 0.1% laurylsarcosine with probes generated from pGEM-T-812 and pTopo-TA-XL-430 plasmids. DIG labeling and chemiluminescent detection were performed as per the manufacturer's instructions (Roche, Germany). Alternatively, radiolabeling of probes using α-^{32}P dCTP (BRIT, India) and detection were performed according to Sambrook *et al.*, 1989.

Sequencing, primer walking and CNV detection: To confirm the fidelity of amplification automated DNA sequencing was performed (ABI – 3130, USA) as per the manufacturer's instructions. Primer walking was initiated with the primers dbo_F and DCP2_P19_R and from the terminal part of the sequence obtained, new primers P19_W2_F 5′- GGAGATCTGTTTGAAATATCTCTTCACATT–3′ and P19_W2_R 5′– GGCGCGTCAGCATTGTTCATACAAAGCTAC-3′ were designed. Long-range PCR with P19_W2 was performed as described previously. Sequence chromatograms were assessed and analyzed with FinchTV 1.4.0, Geospiza Inc. Semi-quantitative assessment of copy number variance (CNV) of the intergenic sequence in $DCP2^{l(3)tb}$ was determined through PCR analyses. A 156 bp sequence (3L: 15826497..15826652) was chosen to be amplified by CNV_F 5′- ACAGTTGGCTCTGTGATAAATGT-3′ and CNV_R 5′- AGTGCAACGGAAGGGAATCT-3′ against an internal control sequence of 153 bp, corresponding to the gene *Dsor*, amplified by the primer pair Dsor_F 5′-CCACCCTGGAGTCGATATTC-3′ and Dsor_R 5′-GTCCTTGAACTCGGTGGAGA-3′. Thermal cycling parameters included an initial denaturation at 95° (5 min) followed by 28 cycles of 30 s at 94°, 30 s at 60°, and 30 s at 72°. Final extension was carried out at 72° for 10 min. The PCR products were electrophoresed on 2% agarose gel with a 100-bp DNA ladder (BR Biosciences, India).

RNA isolation and RT-PCR

For semi-quantitative reverse transcription-polymerase chain reaction (RT-PCR), total RNA was isolated from the 50 brains from wandering late third instar larvae from the genotypes mentioned in the respective cases in the results section, using TRI Reagent following the manufacturer's protocol (Sigma-Aldrich, India). RNA pellets were dissolved in nuclease-free water, followed by treatment with 2U of RNase-free DNaseI (Thermo Scientific, USA) for 40 min at 37°. First strand cDNA was synthesized using 200 U of RevertAid reverse transcriptase (Thermo Scientific, USA) and 80 pmol of oligo(dT)$_{18}$ primer (Thermo Scientific, USA). PCR was carried out for Cyclin A (amplicon size 77 bp), Cyclin E (amplicon size 163 bp) and Diablo (amplicon size 179 bp) using G3PDH (amplicon size 144 bp) as internal control. In either case, the thermal cycling parameters included an initial denaturation at 95° (5 min) followed by 30 cycles of 30 s at 94°, 45 s at 60°, and 1 min at 72°. Final extension was carried out at 72° for 10 min. The PCR products were electrophoresed on 1.8% agarose gel with a 100 bp DNA ladder (BR Biosciences, India). The forward and reverse primers used are listed below.

Forward primers –
Cyclin A 5′–ACGTTTCTCCCTCCATGAGC-3′
Cyclin E 5′–GAGGCGTCAGAAGACTTTCG-3′
Dbo 5′–CACGCTTTCGTATCTCATTTAGTTT-3′
G3PDH 5′–CCACTGCCGAGGAGGTCAACTA-3′

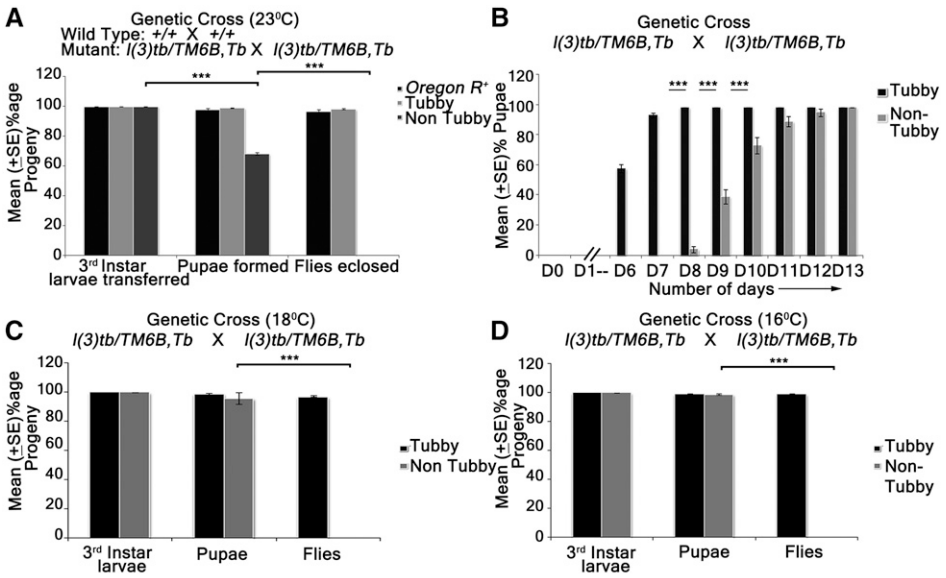

Figure 1 Developmental delay in *l(3)tb* homozygotes. Homozygous *l(3)tb* show delayed larval development with lethality at larval/pupal stage (A, B) and is not a conditional temperature sensitive allele (A, B, C). Homozygous *l(3)tb* progeny, at 23°, showed lethality at larval and pupal stages and no flies eclosed as compared to wild type and heterozygous *l(3)tb* progeny with balancer chromosome (A). Homozygous *l(3)tb* progeny individuals demonstrated extended larval life up to day 12/13 where as heterozygous progeny individuals followed the normal wild type pattern of development (B). (C) and (D) show significant increase in viability of homozygous (non-tubby) *l(3)tb* larvae at lowered temperatures of 18° and 16°, respectively, though there also occurred absolute lethality at pupal stages. Each bar represents mean (± SE) of three replicates of 100 larvae in each. *** indicates $P < 0.005$.

Reverse primers –
Cyclin A 5′–ACTTTGCGACATGCCTGAGA-3′
Cyclin E 5′–AATATTGTCACCGACGACTC-3′
Dbo 5′–GCGAATTTTTGTATAATTGTTGACC-3′
G3PDH 5′–GCTCAGGGTGATTGCGTATGCA-3′

Immunocytochemistry and Immunoblotting

The imaginal discs and/or brain ganglia were collected from wild type *Oregon R*$^+$ wandering 3rd instar larvae, just before pupation (110 h AEL) and in mutant homozygous *l(3)tb* from day 6 and day 10/12. The tissues were processed for immunostaining/immunoblotting as described in Banerjee and Roy 2018, with the desired antibodies. Primary antibodies used in this study were - Anti-Discs large, 4F3 (1:50, Developmental Studies Hybridoma Bank, Iowa,USA), Anti-Armadillo (1:100, a kind gift by Prof LS Shashidhara, IISER Pune, India), Anti-Elav (Rat-Elav-7E8A10, 1:100, DSHB, USA), Anti-DE-Cadherin (DCAD2, 1:20, DSHB, Iowa, USA), Anti-phospho-Histone 3 (1:500, Millipore, Upstate, USA), Anti-Deadpan (1:800, a kind gift from Prof. Volker Hartenstein, University of California, USA) and Anti-Cyclin E (HE12; sc-247, 1:50, Santa Cruz, India). Appropriate secondary antibodies conjugated either with Cy3 (1:200, Sigma-Aldrich, India) or Alexa Fluor 488 (1:200; Molecular Probes, USA) or Alexa Fluor 546 (1:200; Molecular Probes, USA) were used to detect the given primary antibody, while chromatin was visualized with DAPI (4', 6-diamidino-2-phenylindole dihydrochloride, 1μg/ml Sigma-Aldrich, India). Counterstaining was performed with either DAPI (4', 6-diamidino-2-phenylindole dihydrochloride, Sigma-Aldrich, India) at 1μg/ml, or phalloidin-TRITC (Sigma-Aldrich, India) at 1:200 dilutions. Tissues were mounted in DABCO (antifade agent, Sigma-Aldrich, India). The immunostained slides were observed under Zeiss LSM 510 Meta Laser Scanning Confocal microscope, analyzed with LSM softwares and assembled using Adobe Photoshop 7.0.

Statistical analysis

Sigma Plot (version 11.0) software was used for statistical analyses. All percentage data were subjected to arcsine square-root transformation. For comparison between the control and experimental samples, One-Way ANOVA was performed. Data were expressed as mean ± SE of mean (SEM) of several replicates.

Data availability

Supplemental Files are available at figshare. Fly strains are available upon request. The authors affirm that all data necessary for confirming the conclusions are present within the article, figures and tables. Supplementary Figure S6 contains necessary sequence information. Supplemental material available at figshare: https://doi.org/10.25387/g3.12568265.

RESULTS

l(3)tb homozygotes show the classic hallmarks of cancer in Drosophila including developmental delay, abnormal karyotype, larval/pupal lethality along with tumorous brain and wing imaginal disc

Developmental analysis of *l(3)tb* homozygotes showed that while embryos hatched normally and developed alike heterozygous siblings [*l(3)tb/TM6B*], the third instar larvae reached the wandering stage quite late with the larval stage extending up to 12 or 13 days (Figure 1B). Although 66.8% of the larvae survived to pupate (Table 1), they died in the pupal stage following bloating, increase in size and cessation of growth (Figure 1A). Hence, the mutation is lethal, with the lethality being pronounced in the pupal stage. Lowering the temperature to 16° or 18° reduced the larval mortality, causing 96% of larvae to pupate but did not improve pupal survival (Figure 1 C and D). Analysis of larval brain and imaginal discs in the homozygotes in the early (Day 6) and late (Day 10-12) larval phase showed gross morphological alterations in the size of the larval brain, wing and eye imaginal discs (Figure 2A–G) as compared to the wandering wild type third instar larvae (115 h **a**fter **l**arval **h**atching [ALH]). The brain was smaller in size than the wild type (*Oregon R*$^+$), or heterozygous [*l(3)tb/TM6B*] individuals till 115 h ALH but started showing aberrant growth in the dorsal lobes thereafter, with significant differences in the diameter and area

Table 1 Homozygous mutation in *l(3)tb* causes larval and pupal lethality

Genetic cross (23°C ± 1)	Total Eggs	No. of eggs hatched	3rd Instar larvae transferred	Pupae formed	Flies eclosed
l(3)tb/TM6B	1500	972	Non-Tubby-	Non-tubby	Non Tubby
X *l(3)tb/TM6B*		(O= 64.8%)	468	313	0
		(E = 66.7%)	(O = 48.1%)	(O = 66.8%)	
			(E= 50%)		
			Tubby	Tubby	Tubby
			473	468	465
			(O= 48.6%)	(O = 98.9%	(O = 99.4%)
			(E = 50%)	(E = 100%)	(E = 100%)

Numbers in parenthesis indicate the percentage observed (O) and expected (E) values out of the total progeny from previous stage.

of the lobes. There was no loss of symmetry in the overgrown brain hemispheres in most of the cases, except in some cases where they were deformed and fused with the imaginal discs (Figure 2 J and K). A similar trend in morphological aberration was observed in the wing discs, which remained small initially, but later enlarged sufficiently (Figure 2L), with an abnormal protrusion in the wing pouch. Analysis of mitotically active cell population by staining for phosphorylated histone 3 (PH3), revealed an increased number of active mitoses in the homozygous mutant brains (Figure 3A-O; 3V) and wing discs (Figure 3P-V) (Day 6) in comparison to the wild type; the number increased with increase in age of the mutant. However, mitotic karyotypes of the mutant brain lacked numerical aberrations, despite showing extensive variability in condensation (Figure 2 H and I).

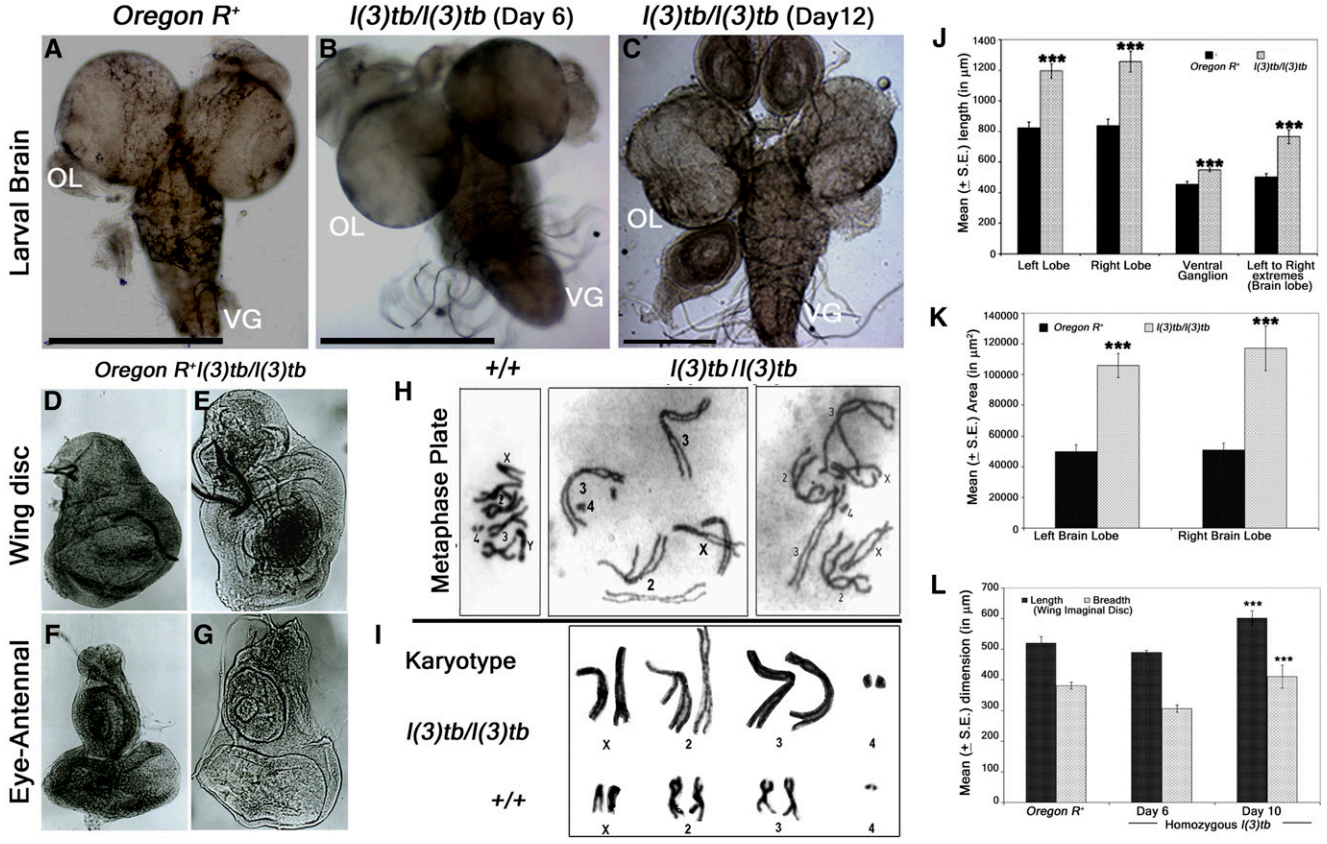

Figure 2 Morphological and chromosomal alterations in *l(3)tb* homozygotes. Homozygous *l(3)tb* mutants show severe morphological alteration in delayed 3rd instar larval brain, wing and eye-antennal disc. Homozygous *l(3)tb* mutant 3rd instar larvae revealed tumorous brain of day 12 (C) as compared to day 6 of homozygous mutant (B) and day 5 of wild type, *Oregon R*$^+$ (A). *l(3)tb* homozygotes exhibited highly significant differences in the overall circumference of the left and right brain lobes in the delayed stage (day 10) as compared to the respective wild type brain lobes (J). Significant differences were found in the area (μm^2) of respective brain lobes of *l(3)tb* homozygotes and wild type (K). Dimensions of wing and eye-antennal imaginal discs of delayed 3rd instar larvae from homozygous *l(3)tb* mutant revealed significant increase in size (D,E,F,G). Length and breadth of wing discs from 3rd instar larvae of *l(3)tb* mutant of day 6 were found to be smaller than the wing imaginal discs from wild type, but wing discs from extended larval period (day 10) showed significant increase in size (L). Metaphase chromosome preparation of brain cells (H) from wild type and *l(3)tb* homozygotes exhibited abnormal karyotypes (I) where *l(3)tb* homozygotes showed less condensed and extended chromosome morphology as compared to wild type, *Oregon R*$^+$. *** denotes $P < 0.005$.

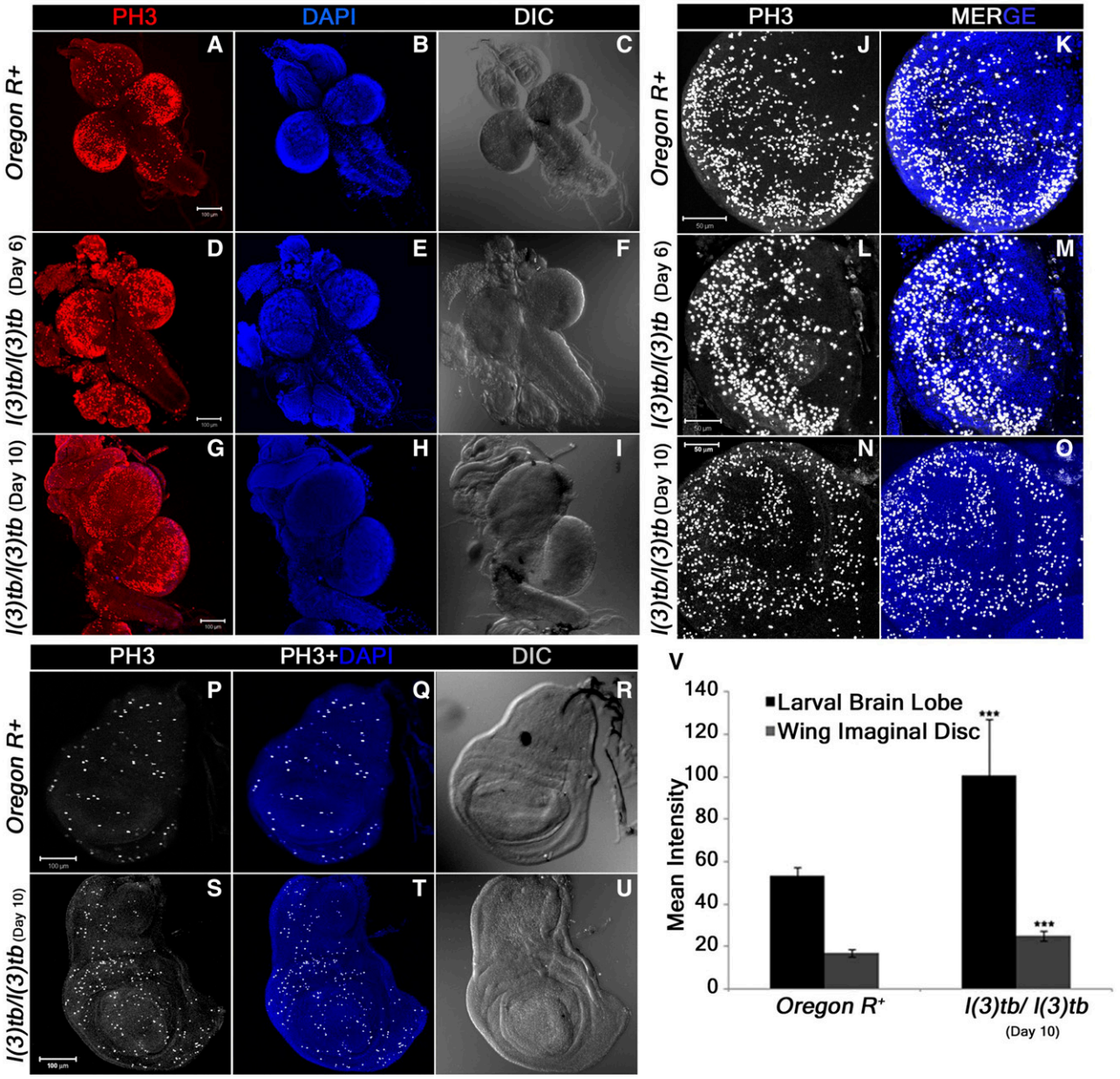

Figure 3 Tumorous tissues in *l(3)tb* homozygotes show enhanced mitotic potential. Enhanced mitotic potential observed in the tumourous tissues of homozygous *l(3)tb* as shown in larval whole brain (A), brain lobes (D, G) and wing imaginal discs (S) immunostained for PH3, a potent mitotic marker. Distribution of PH3 labeled cells counter stained with DAPI cells in wild type (A) and homozygous *l(3)tb* (Day 6 and Day 10) larval brain (D, G) and also in wild type brain lobes (B, C) and homozygous mutant brain lobes (E, F for day 6; H, I for day 10) indicated high mitotic index as compared to wild type. Similarly, more mitotic positive cells were seen in tumorous wing imaginal discs (day 10) of homozygous mutant *l(3)tb* (S) as compared to wild type, *Oregon R*$^{+}$ (P) . DIC images (C, F, I and R, U) illustrate external normal morphology in wild type and more pronounced tumorous phenotypes in homozygous *l(3)tb* larval brain and wing imaginal discs. Quantitative analysis showed increase in the number of mitotic positive cells in homozygous mutant larval brain lobes and wing imaginal discs as compared to wild type and the difference was highly significant (V). The images are projections of optical sections acquired by confocal microscopy. Staining was done in triplicates with 10 brains and 15 wing imaginal discs in each group. Significant difference is represented as *** $P \leq 0.005$ using one-way ANOVA.

Eye-antennal discs and leg imaginal discs also show morphological and developmental anomalies in l(3)tb homozygous individuals

Global analysis of morphological aberrations in the mutant homozygotes showed that besides the tumorous brain and wing imaginal discs, eye-antennal discs and leg imaginal discs were also overgrown with a transparent appearance. Expression of Elav and Dlg in the eye-antennal discs revealed similarities to the developmental perturbations observed in the wing discs and brain (Figure 4S, V). In the early third instar mutant larvae (Day 6), all photoreceptor cells showed expression of Elav, similar to the wild type tissue (Figure 4J and N). However, during advanced stages of larval tumorigenesis (Day 10), it dwindled eventually (Figure 4R). The Elav expressing cells, posterior to the morphogenetic furrow, co-express Dlg and demonstrate the typical ommatidial

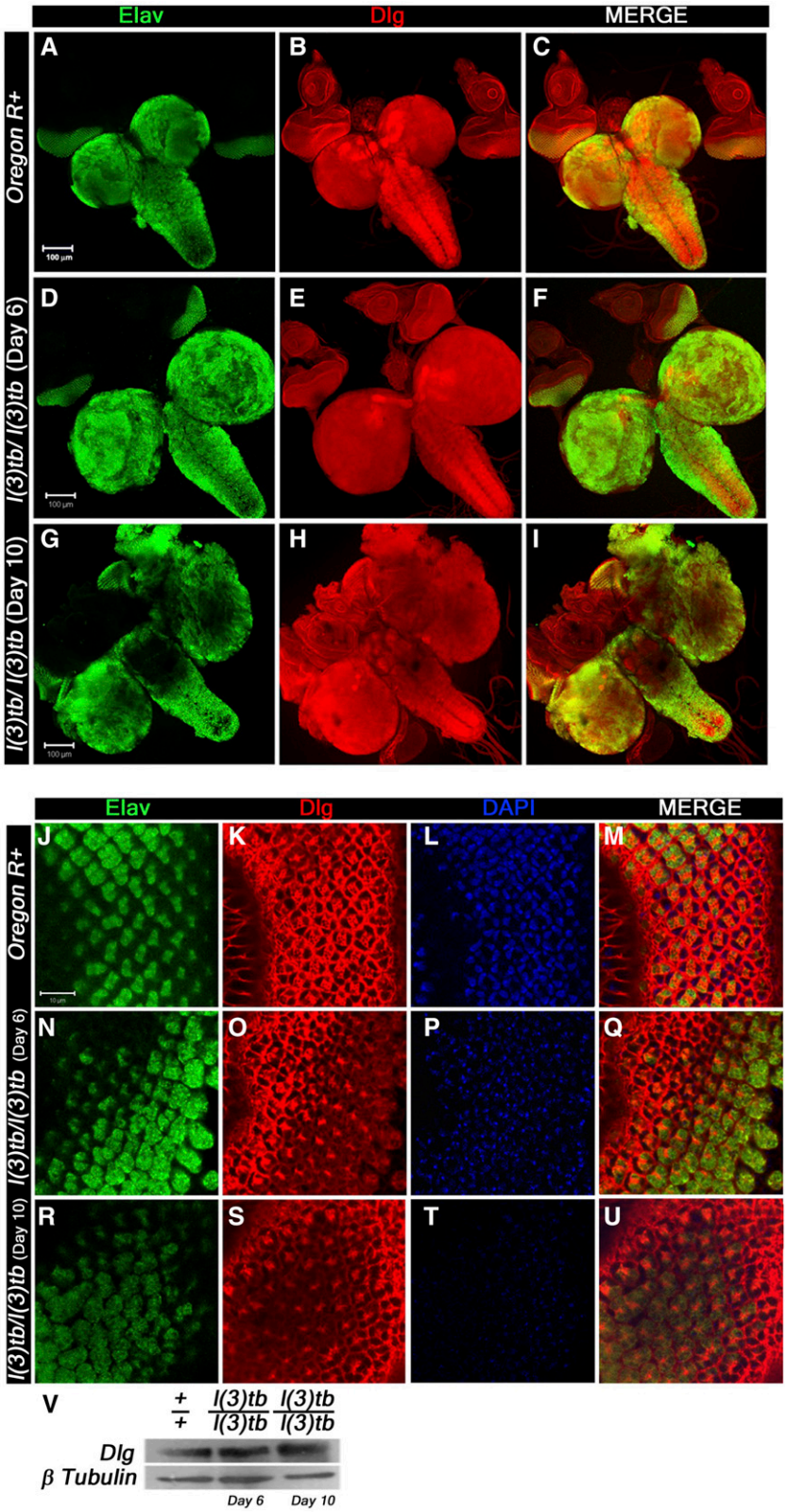

Figure 4 *l(3)tb* mutants show progressive loss of mature neurons along with increase in junction proteins. Confocal photomicrograph show loss of mature neurons and increase in junction protein, Dlg, in delayed (Day 10) homozygous *l(3)tb*. 3rd instar larval brain shows intense staining of Elav (green) in day 6 (D) of homozygous mutant later on show loss of staining in enlarged brain of day 10 (G), while the wild type brain (A) showed normal pattern of Elav staining. Dlg stained the ventral nerve chord and central brain in optic lobes of wild type (B), which is similar to that observed in day 6 of homozygous mutant brain (E) but in delayed larval brain, (day 10), the pattern was altered (H). Scale shown is 100µm. Neuronal tissue from eye imaginal discs also display loss of neurons seen through Elav staining in day 10 (R) as compared to day 6 (N) in homozygous *l(3)tb* mutant as well as to wild type (J). Pattern of junctional protein, Dlg, in eye imaginal discs is also altered in day 10 (S, V) as compared to day 6 (O) and wild type (K). Counter stain with DAPI shows very weak intensity in day 10 (T) reflecting disintegrating chromatin as compared to day 6 (P) and wild type (L). Scale bar represents 10 µm.

arrangement. In the mature mutant larvae, however, the eye discs demonstrate significant deviations from the usual regular arrangement of ommatidia. The leg imaginal discs, which reside close to the brain and wing imaginal discs also show enlargement in size that increases with advancement of larval stage. They show gradual disruption of normal expression of DE-cadherin and Armadillo (Figure 5), alike tumorous wing discs (see above), implying the mutation and subsequent tumor to affect developmental homeostasis in adjacent tissues as well.

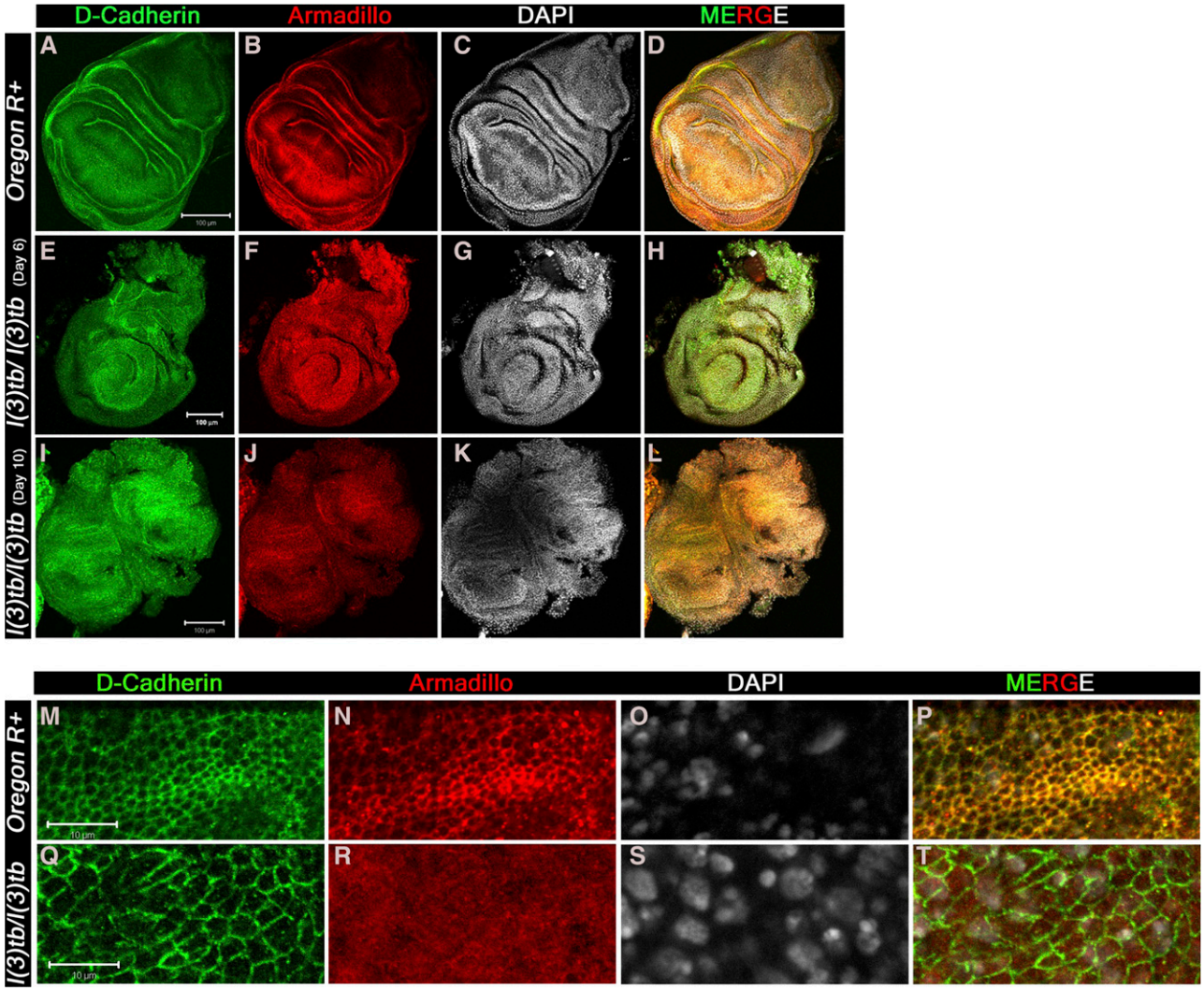

Figure 5 Tumor caused in the homozygous *l(3)tb* mutant completely alters the distribution patterns of DE-cadherin and Armadillo. Confocal images of 3rd instar larval wing imaginal discs immunolabeled to visualize the altered distribution pattern of cadherin-catenin complex proteins. Tumor caused in the homozygous *l(3)tb* mutant completely altered the distribution pattern of both, *trans*-membranous protein DE-cadherin (A, E, I, M, Q) and Armadillo (β-Catenin, B, F, J, N, R) adherens junction proteins. Alteration of both proteins is more pronounced in the wing imaginal discs from mutant larva during extended larval life (I, J) than in the early wing imaginal disc (E, F) as compared to distinct pattern of DE-cadherin (A) and Armadillo (B) in the wild type wing imaginal discs. Armadillo is a binding partner of *trans*-membranous protein DE-cadherin having roles in cell adhesion and regulate tissue organization and morphogenesis. Merged images also substantiate the altered distribution of both junctional proteins in the homozygous mutant (H, L) as compared to the wild type (D) where co-localization is indicated by yellow pattern. Higher magnification of wing imaginal disc (pouch region) demonstrate altered distribution pattern of DE-cadherin (Q) and Armadillo (R) in homozygous *l(3)tb* mutant as compared to wild type (N, R). Increase in cell size seen in homozygous *l(3)tb* mutant (Q) as compared to wild type (M). Complete loss of Armadillo staining observed in homozygous *l(3)tb* (R) whereas normal pattern seen in wild type wing disc (N). Chromatin size also altered in homozygous *l(3)tb* (S) as compared to wild type (O). Wild type shows clear co-localization of DE-cadherin and Armadillo (P), while there is complete loss of co-localization in homozygous *l(3)tb* wing imaginal discs (T). Scale bar represents 100 μm (A to L) and 10 μm (M to T).

Genetic mapping through meiotic recombination and complementation mapping identify l(3)tb to be allelic to DCP2

The mutation *l(3)tb*, being recessive and on the third chromosome, was maintained with *TM6B* balancer. Analysis of meiotic recombination frequencies of an unmapped mutation with known markers is a classical technique that has been routinely employed to identify its cytogenetic position. In order to bring *l(3)tb* in a chromosome with such markers (*ru cu ca*), we allowed meiotic recombination to occur between *l(3)tb* and the eight recessive markers present on the "*rucuca*" chromosome (Table 2). 113 recombinant males were observed and recombination frequencies were calculated in centiMorgan (cM). Table 3 shows the recombination frequencies of each marker (locus) with the mutation *l(3)tb*. Preliminary analysis suggested that *l(3)tb* was close to *thread* (*th*) with minimum recombination events between the two loci (2.65%). Further analysis of recombination events between *h-l(3)tb* [17.78%], *st-l(3)tb* [1.23%] and *cu-l(3)tb* [8.29%] (Table 4) and comparing with the positions of each of the markers, the mutation was estimated to be located left of *thread* (43.2 cM; band 72D1) between 41.71 cM–42.77 cM, *i.e.*, at the cytological position 71F4-F5.

Table 2 Rearranged genotypes of 113 males after various recombination events between all the eight visible markers of *rucuca* chromosome

S.No.	Genotypes								No. of Flies	Status of *l(3)tb* locus	
1.	*ru*	*h*	*th*	+	+	+	+	+	1	1 l^+	
2.	*ru*	*h*	*th*	*st*	+	+	+	+	1	1 l^+	
3.	*ru*	*h*	*th*	*st*	*cu*	+	+	+	1	1 l^+	
4.	*ru*	*h*	*th*	*st*	*cu*	*sr*	+	+	1	1 l^+	
5.	*ru*	*h*	*th*	*st*	*cu*	*sr*	*e*	+	3	3 l^+	
6.	*ru*	*h*	*th*	*st*	*cu*	*sr*	*e*	*ca*	6	6 l^+	
7.	+	*h*	*th*	*st*	*cu*	*sr*	*e*	*ca*	6	6 l^+	
8.	+	+	*th*	*st*	*cu*	*sr*	*e*	*ca*	6	6 l^+	
9.	+	+	+	*st*	*cu*	*sr*	*e*	*ca*	1	1 *l*	
10.	+	+	+	+	*cu*	*sr*	*e*	*ca*	2	1 *l*	1 l^+
11.	+	+	+	+	+	*sr*	*e*	*ca*	2	2 *l*	
12.	+	+	+	+	+	+	*e*	*ca*	4	4 *l*	
13.	+	+	+	+	+	+	+	*ca*	6	6 *l*	
14.	+	+	+	+	+	+	+	+	26	26 *l*	
15.	*ru*	*h*	+	+	+	+	+	+	6	6 *l*	
16.	*ru*	+	+	+	+	+	+	+	6	6 *l*	
17.	*ru*	+	+	+	+	+	+	*ca*	3	3 *l*	
18.	*ru*	+	+	+	+	+	*e*	*ca*	1	1 *l*	
19.	*ru*	*h*	+	+	+	+	+	*ca*	7	7 *l*	
20.	*ru*	*h*	+	+	+	*sr*	*e*	*ca*	5	5 *l*	
21.	*ru*	+	+	+	+	*sr*	*e*	*ca*	3	3 *l*	
22.	*ru*	*h*	+	+	*cu*	*sr*	*e*	*ca*	1	1 *l*	
23.	*ru*	*h*	*th*	*st*	*cu*	+	*e*	*ca*	1	1 l^+	
24.	+	+	*th*	*st*	*cu*	*sr*	+	*ca*	1	1 l^+	
25.	+	+	*th*	*st*	*cu*	*sr*	*e*	+	3	3 l^+	
26.	+	+	*th*	*st*	+	+	+	+	1	1 l^+	
27.	+	+	+	+	+	*sr*	*e*	+	1	1 l^+	
28.	+	*h*	+	+	+	+	+	+	1	1 l^+	
29.	+	*h*	*th*	*st*	*cu*	*sr*	*e*	+	5	4 l^+	1 *l*
30.	+	*h*	*th*	*st*	*cu*	*sr*	+	+	1	1 l^+	
31.	+	*h*	*th*	*st*	*cu*	+	+	+	1	1 l^+	
Total									113		

Complementation analysis with molecularly defined Drosdel and Exelixis deficiency lines (N = 85), spanning the entire chromosome 3, identified four lines which failed to complement the mutation, *viz*., *Df(3L)BSC774*, *Df(3L)BSC575*, *Df(3L)BSC845* and *Df(3L)RM95*, which was generated in the lab using progenitor RS stocks. Trans-heterozygotes *l(3)tb*/*Df(3L)BSC575* were pupal lethal and the dying non-tubby larvae showed phenotypes similar to *l(3)tb* homozygotes, suggesting the mutation to reside between 71F1

Table 3 Recombination frequencies (RF) between various recessive markers on *rucuca* chromosomes (*roughoid, hairy, thread, scarlet, curled, stripe, ebony*, and *claret*) and *l(3)tb*

Sl. No.	Association of marker with *l(3)tb*	Flies						Recombination frequency (RF) $\frac{R}{P+R}\times 100$
		Parental (P)			Recombinant (R)			
		Genotype	No. of flies		Genotype	No. of flies		
1.	*ru* - *l*	ru^+ *l* *ru* l^+	18 44	62	ru^+ l^+ *ru l*	18 33	51	45.13
2.	*h* - *l*	h^+ *l* *h* l^+	54 25	79	h^+ l^+ *h l*	12 22	34	30.08
3.	*th* - *l*	th^+ *l* *th* l^+	74 36	110	th^+ l^+ *th l*	1 2	3	2.65
4.	*st* - *l*	st^+ *l* *st* l^+	73 35	108	st^+ l^+ *st l*	2 3	5	4.42
5.	*cu* - *l*	cu^+ *l* *cu* l^+	71 34	105	cu^+ l^+ *cu l*	3 5	8	7.07
6.	*sr* - *l*	sr^+ *l* *sr* l^+	62 32	94	sr^+ l^+ *sr l*	4 15	19	16.8
7.	*e* - *l*	e^+ *l* *e* l^+	56 30	86	e^+ l^+ *e l*	7 20	27	23.89
8.	*ca* - *l*	ca^+ *l* *ca* l^+	42 32	74	ca^+ l^+ *ca l*	16 33	49	43.3

Table 4 Recombination events between *h-l*, *st-l* and *cu-l*

S.No.	Association of marker with *l(3)tb*	Flies				Recombination frequency $\frac{R}{P+R}\times 100$
		Parentals (P)		Recombinants (R)		
		Genotype	No. of flies	Genotype	No. of flies	
1.	*h - l*	h^+ *l*	89	h^+ l^+	18	17.78
		h l^+	185	*h l*	40	
			96		22	
2.	*st - l*	st^+ *l*	252	th^+ l^+	2	1.23
		st l^+	480	*th l*	6	
			238		4	
3.	*cu - l*	cu^+ *l*	269	ru^+ l^+	22	8.29
		cu l^+	552	*ru l*	50	
			283		28	

and 72A1 on the left arm of chromosome 3. Further analysis using six deletion lines belonging to the above region (71F1–72A2) identified the mutation to reside between 71F4 to 71F5, which, strangely, is a gene desert region. Complementation analyses performed with lethal insertion alleles (N = 26) of genes residing proximal or distal to 71F4-F5 identified two lethal *P*-element insertion alleles of *DCP2* (mRNA decapping protein 2; CG6169), *viz.*, *P{GT1}DCP2*^{BG01766} and *PBac{RB}DCP2*^{e00034}, which failed to complement the *l(3)tb* mutation (Figure 7A and C), as well as those deletions which had failed to complement *l(3)tb*, implying the mutation to be allelic to *DCP2* (72A1).

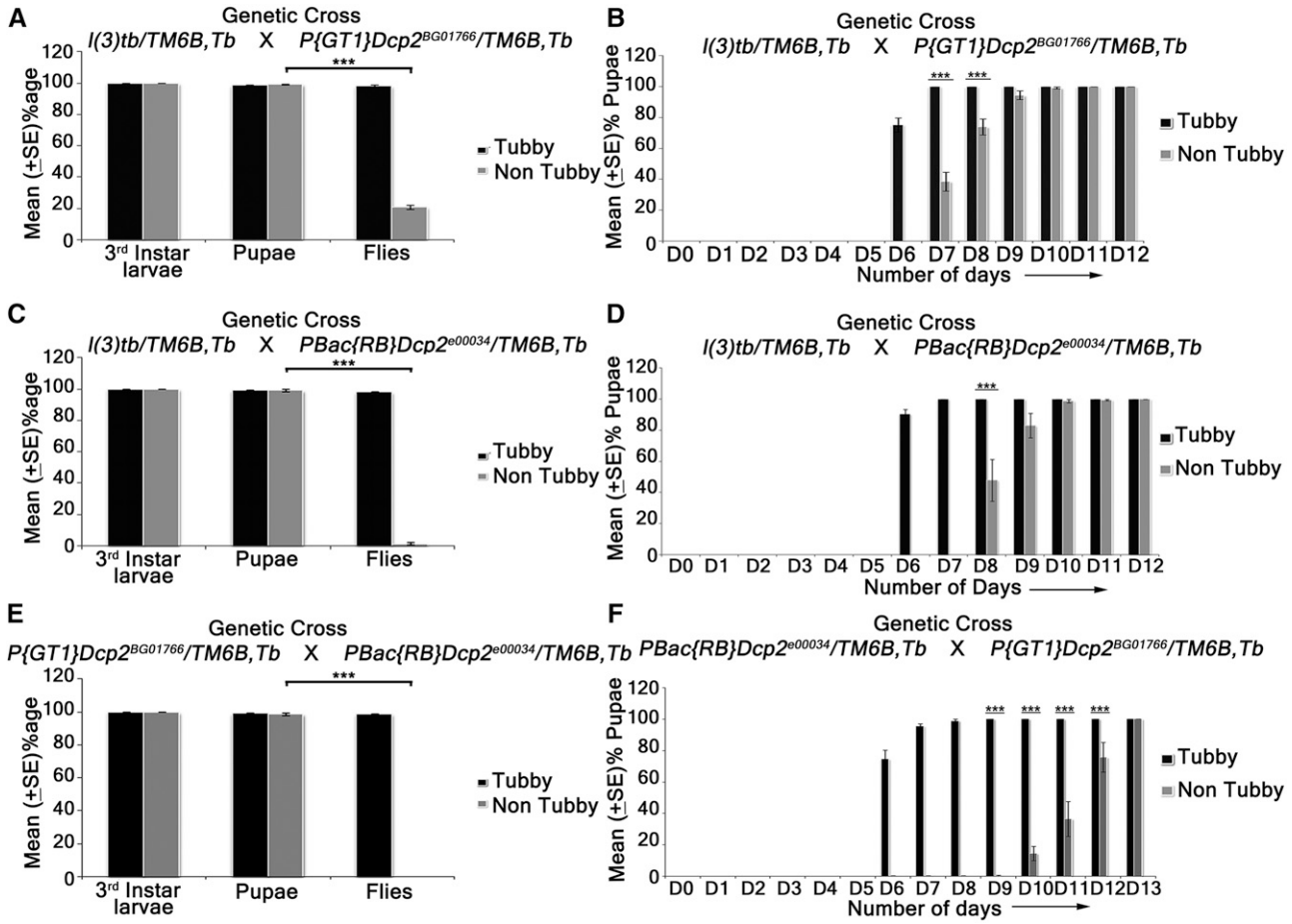

Figure 6 Trans-heterozygotes of *DCP2* mutants and *l(3)tb* show developmental delay and larval/pupal lethality. Viability assay performed on various hetero-allelic combinations between alleles of *DCP2* and the mutation in *l(3)tb*. Homozygous *l(3)tb* exhibited larval as well as pupal lethality. 69% of homozygous larvae pupated whereas no fly eclosed from the pupae. *l(3)tb trans*-heterozygous with *P{GT1}-DCP2*^{BG01766} showed only 18.4% fly eclosed (A). *l(3)tb/ PBac{RB}DCP2*^{e00034} *trans*-heterozygote (C) causes 100% lethality at pupal stage. Trans-allelic combination *P{GT1}DCP2*^{BG01766}*/ /PBac{RB}DCP2*^{e00034} (E) also exhibited 100% pupal lethality. Developmental delay seen in *trans*-heterozygotes *l(3)tb /P{GT1}DCP2*^{BG01766} (B) and *l(3)tb/PBac{RB}DCP2*^{e00034} (D) as in homozygous *l(3)tb*. Progeny from heterozygous for both the alleles of *DCP2* gene, *PBac{RB}DCP2*^{e00034} */P{GT1}DCP2*^{BG01766} (F) also exhibited developmental delay. *** indicates $P < 0.005$.

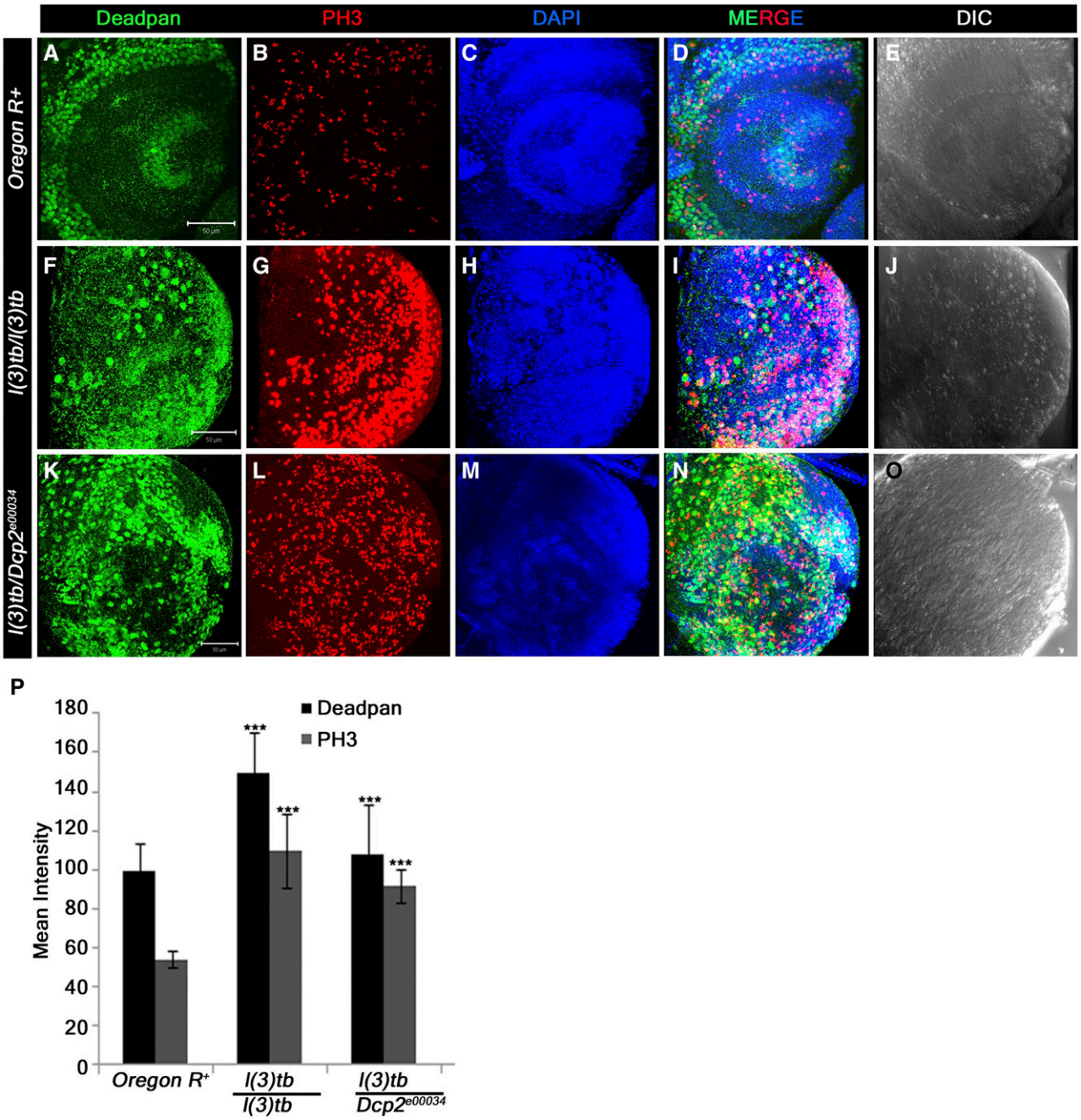

Figure 7 Trans-heterozygotes of *DCP2* mutants and *l(3)tb* show tumorous larval brain with elevated neuroblast numbers. Heterozygous combination of *l(3)tb* with $DCP2^{e00034}$ allele resulted in significant increase in the number of neuroblasts and mitotically active cells. Confocal projections showing immunolocalisation of Deadpan, a neuroblast marker (Green, A, F, K) and PH3 (red, B, G, L) marking the mitotic cells, show enhanced neuroblast population in homozygous mutant (F) and in heterozygous *l(3)tb* with $DCP2^{e00034}$ allele (K). Similarly, increased number of mitotic cells (PH3 positive) are also observed in heterozygous *l(3)tb* with $DCP2^{e00034}$ allele (L), similar to homozygous *l(3)tb* mutant (G). Quantitative analyses of NBs and mitotically active cells show significant differences when compared with the wild type (P). *** $P < 0.005$. Scale bar indicates 50 μm.

Trans-heterozygotes of DCP2 mutants and l(3)tb show developmental delay, tumorous larval brain with elevated neuroblast numbers, larval/pupal lethality and developmental defects in escapee flies

Trans-heterozygotes of *l(3)tb* with two known alleles of *DCP2*, *viz.*, $P\{GT1\}DCP2^{BG01766}$ and $PBac\{RB\}DCP2^{e00034}$, showed developmental delay and third instar larvae persisted in the same stage till Day 10 ALH (Figure 6B and D), and showed tumorous phenotypes of brain and wing imaginal discs (Supplementary Figure S4), similar to the *l(3)tb* homozygotes. The expression of Deadpan (Dpn), a marker for neuroblasts, shows an increased number of neuroblasts in the larval brain of the *trans*-heterozygotes as well as *l(3)tb* homozygotes (Figure 7F, K and P). Also, the *trans*-heterozygous progeny showed a higher mitotic index than the wild-type progeny, similar to the *l(3)tb*

Table 5 Fertility assay of *trans*-heterozygotes *P{GT1}DCP2^{BG01766}/l(3)tb* demonstrating male and female sterility

Cross	*l(3)tb/P{GT1}DCP2^{BG01766}* (males) X +/+ (Virgin females)	*l(3)tb/P{GT1}DCP2^{BG01766}* (Virgin females) X +/+ (males)
Total No. of Pair Mating	70	83
Fertile	28 (40%)	18 (21.7%)
Sterile	42 (60%)	55 (66.3%)

homozygotes (Figure 7G, L and P). While *PBac{RB}DCP2^{e00034}/l(3)tb* was found to be 100% pupal lethal, *P{GT1}DCP2^{BG01766}/l(3)tb* was only 81.6% lethal (Figure 6A and B), with the rest 18.4% pupae eclosing as flies. However, the escapee flies showed several developmental abnormalities, *viz.*, defects in the wing (9.5%), thorax closure (3.2%), loss of abdominal para-segments and abdominal bristles (3.2%), and presence of melanotic patches (22.2%), leg defects (41.3%) or eclosion defects (12.7%) (Supplementary Figure S2). Analysis of compound eyes in these escapees revealed complete loss of regular arrangement of ommatidia and ommatidial bristles

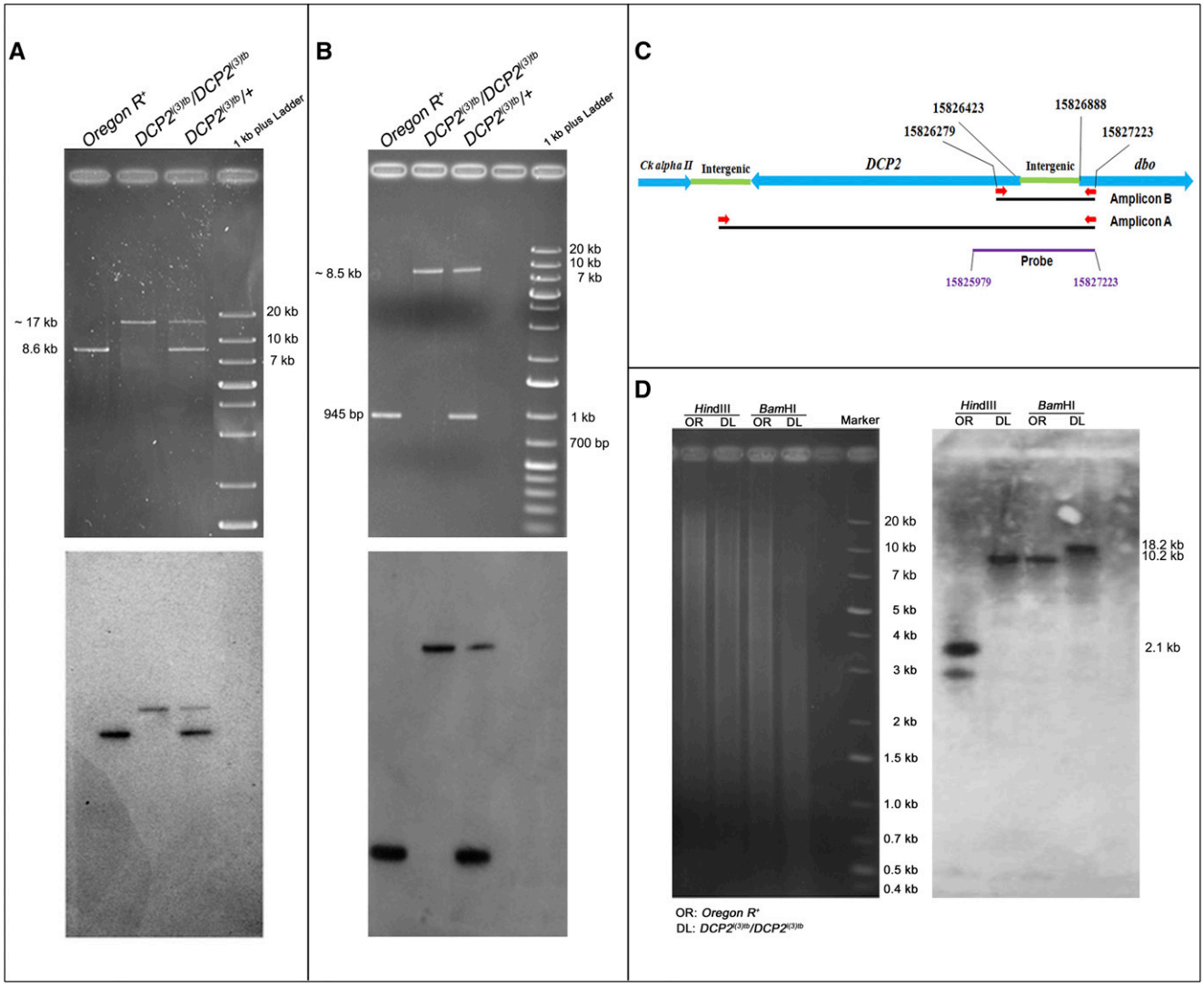

Figure 8 *DCP2$^{l(3)tb}$* is an insertion allele of *DCP2*. Gel electrophoretogram showing the PCR analysis of the full-length *DCP2* (A) and candidate region (B) in the wild type, mutant and the heterozygote. The schematic in C shows the gene arrangement along the chromosome along with the important coordinates. The primers are indicated by red arrows. Amplification of the full length gene shows that the wild type amplicon is of 8.6 kb while the mutant amplicon is sized ~17 kb (A, upper half), whereas the wild type amplicon for the candidate region is of 945 bp while the mutant amplicon is sized ~8.5 kb (B, upper half). The heterozygote harbors both the alleles (wild type and mutant) and thus shows both the amplicons. The lower half in both A and B shows the the blot of the same probed with the pGEM-T-812 probe which spans the candidate mutated region in *DCP2* and is represented by the purple line. D shows the gel electrophoretogram and Southern blot of *DCP2* in the wild type and mutant genome. *Hin*dIII digested genomic DNA showed banding at ~2.1 kb in the wild type genome as against ~10 kb in the mutant genome, the size difference being almost in agreement with the banding profile exemplified by *Bam*HI digestion, with the wild type genome hybridizing at ~10.2 kb and the mutant at ~18 kb.

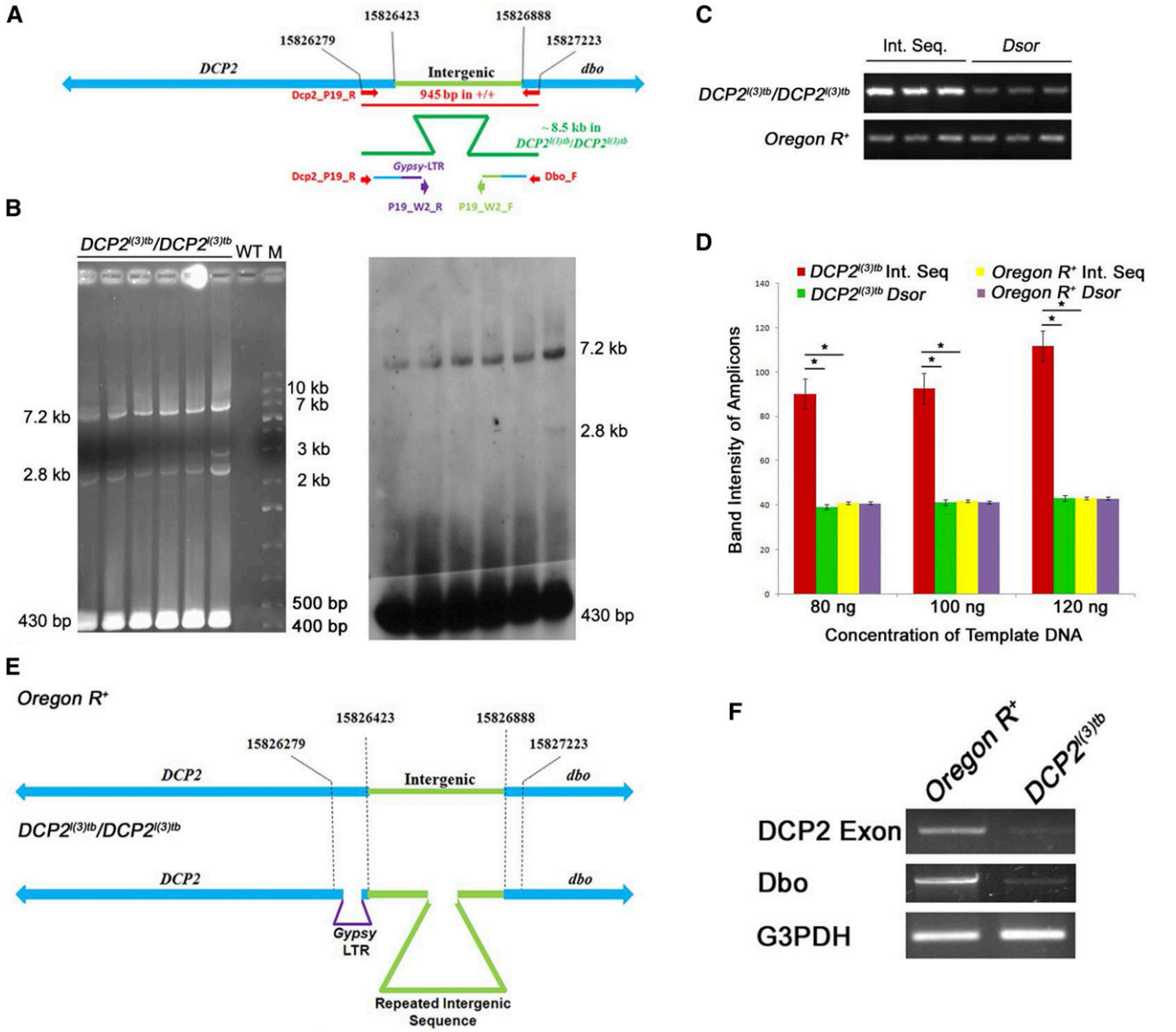

Figure 9 The *DCP2*$^{l(3)tb}$ genome harbors *Gypsy*-LTR like sequence in 5′UTR coding region of *DCP2* and expansion of adjacent upstream intergenic AT-rich sequence along with low expression of the neighboring gene, *dbo*. Gel electrophoretogram showing PCR amplification profile obtained by the primers used (P19_W2_R and P19_W2_F) for the "second step" of walking (B). The alignments of the sequences uncovered in the "first step" are shown as thin lines colored as per homology with the wild type sequence. The region amplified here lies subsequent to the sequence uncovered by the initial primers (A; Dbo_F and Dcp2_P19_R, shown in red arrows). Mentioned alongside the electrophoretogram are the semi-logarithmic estimates of the amplicon size. Shown alongside is the blot of the same hybridized with the probe generated from the ~430 bp amplicon. Semi-quantitative PCR to detect change in copy number of the intergenic region in the *DCP2*$^{l(3)tb}$ genome (C) shows increased amplification of the intergenic sequence in *DCP2*$^{l(3)tb}$ genome as compared to the *Dsor* (control) amplicons in both the genomes. Shown in D is a histogram comparing the fluorescence intensity of PCR amplicons obtained from amplification of the intergenic sequence and the control sequence from the *DCP2*$^{l(3)tb}$ genome and the wild type genome. The schematic in E shows the architecture of the mutant allele, *DCP2*$^{l(3)tb}$ based on the results obtained from fine mapping. Semi-quantitative RT-PCR analyses of transcription from *DCP2* and *dbo* in the wild type and *DCP2*$^{l(3)tb}$ homozygotes (F) shows decreased titer of mRNA from both genes in the tumorous individuals.

(Supplementary Figure S3). Abnormal external genitalia were also observed in the male escapees (data not shown). Subsequent analysis showed that the *trans*-heterozygous escapee flies had compromised fertility, with only 40% of the males and 21.7% of the females being fertile (Table 5).

The similarity in the pattern of development and the defects associated between the *l(3)tb trans*-heterozygotes and homozygotes provide strong genetic proof of allelism between *l(3)tb* and *DCP2*.

DCP2$^{l(3)tb}$ is an insertion allele of DCP2

Fine mapping, performed by overlapping PCR, identified the region (Supplementary Figure S5), amplified by the primer pair, Dbo_F, and DCP2_P19_R, to span the candidate region. The region, which is 945 bp (3L: 15826279..15827223) in the wild type and comprises of 5′UTR coding region of *DCP2*, the adjacent intergenic region and the proximal part of the neighboring gene, *dbo*, showed absence of amplification in the DNA of *l(3)tb* homozygotes, highlighting it as

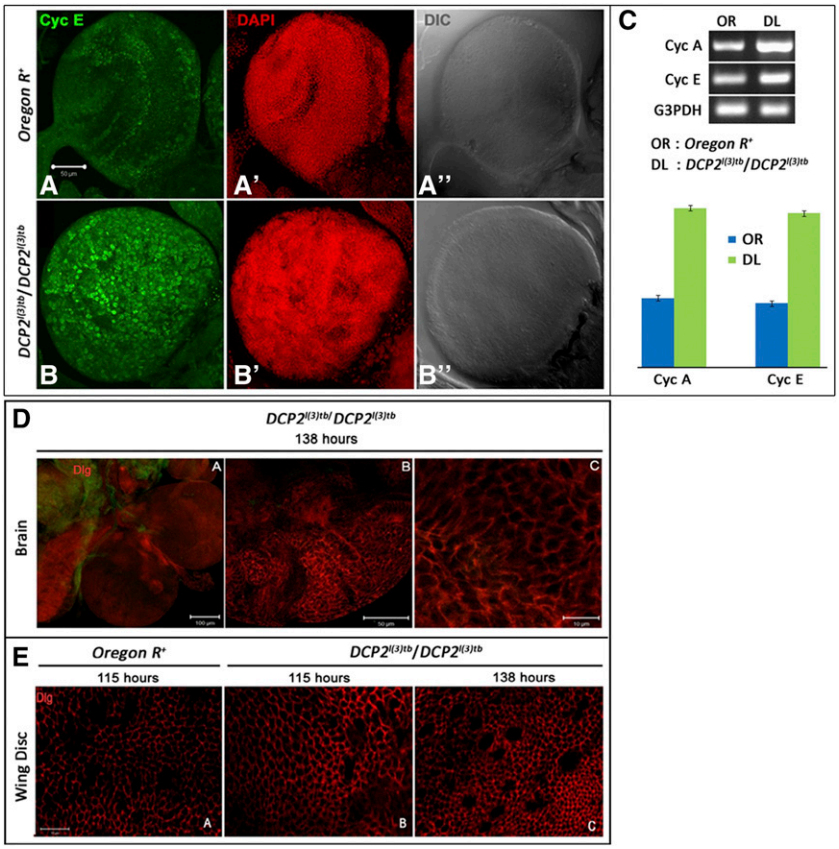

Figure 10 The tumor caused by *DCP2* is hyperplastic with elevated Cyclin A and E. Immunolocalisation of Cyclin E shows elevated expression in the tumorous larval brains of $DCP2^{l(3)tb}$ homozygotes (B) as compared to the wild type (A). Semi-quantitative analyses of mRNA expression of Cyclins A and E show similar elevation in the brain of $DCP2^{l(3)tb}$ homozygotes (C). Expression of Discs-large in the brain (D) and wing discs (E) of the tumorous individuals did not show appreciable loss. At 138h AEL, the wing discs showed increase in cell number concomitant with decrease in cell size (E.C) whereas, at the same stage, the tumorous brain shows increased number of cells at in the optic lobe (D).

the candidate lesion. Long-range PCR using the same pair of primers revealed a large amplicon of ~8.5 kb in the mutant against the 945 bp amplicon in the wild type genome, subjected to the same thermal cycling parameters (Figure 8B). Amplification of the full-length gene *DCP2* using primers residing outside the gene revealed a large amplicon of ~17 kb from the mutant genome as against the 8.6 kb (3L: 15811576..15820204) wild type amplicon (Figure 8A). The pGEM-T-812 probe, which corresponds to the candidate region in the wild type, hybridized with all the amplicons implying the fidelity of amplification (Figure 8A and B). This was further corroborated by the sequencing of the amplicon terminals (data not shown). Southern hybridization of wild type and mutant genomic DNA with *Hin*dIII and *Bam*HI enzymes with pGEM-T-812 probe showed completely different banding profiles. While the *Hin*dIII digested DNA showed a band at ~2.1 kb in the wild type genome, the *l(3)tb* genome showed a single band at ~10 kb, the size difference being almost in agreement with the banding profile exemplified by *Bam*HI digested DNA, wherein, the wild type genome showed a band at ~10.2 kb and the mutant at ~18 kb (Figure 8D). These results imply the presence of an insertion in *DCP2* gene, suggesting that *l(3)tb* is essentially an insertion allele of DCP2. Henceforth *l(3)tb* will be referred to as, $DCP2^{l(3)tb}$.

The $DCP2^{l(3)tb}$ genome harbors Gypsy-LTR Like sequence in 5′UTR coding region of DCP2 and expansion of adjacent upstream intergenic AT-rich sequence

To identify the functional genomics of mutations, it is essential to deduce the nucleotide sequence of the mutation. Thus a convergent bi-directional primer-walk was initiated with the primer pair, which identified the insertion in *DCP2* in the *l(3)tb* genome. On sequencing, the *DCP2*-proximal end showed the presence of wild type sequence till 3L: 15826410 after which a 444 bp AT-rich sequence was detected (Supplementary Figure S6 B-1), which did not show any resemblance with the wild type sequence present at the region whereas the *dbo*-proximal end showed complete wild type sequence profile (3L: 15827143..15826738) (Supplementary Figure S6 B-2). On a homology search to identify the novel sequence obtained, the sequence showed homology with the *Gypsy* LTR sequence of *Drosophila*. On searching for *DCP2* promoters in the Eukaryotic Promoter Database, SIB and aligning the sequence coordinates of the 444 bp insertion, it was found that the insertion is downstream to the transcription start site (TSS) of *DCP2*, which is at 3L: 15826420. Subsequently, long-range PCR was first performed with $DCP2^{l(3)tb}$ and wild type genomic DNA with a new pair of primers from the distal part of the reads obtained above,. Although no amplification was observed with the wild type DNA, the $DCP2^{l(3)tb}$ DNA showed amplicons of sizes ~7.2 kb, ~3 kb, ~2.8 kb and ~430 bp with the 430 bp amplicon showing the highest concentration as observed from the electrophoretogram (Figure 9B). This amplification profile resembled that of tandem repeat bearing regions. To confirm the repetitive nature of the sequence, Southern hybridization was performed with the same electrophoretogram. The 430 bp amplicon was eluted from the gel, cloned in pGEM-T vector and used as a probe. The probe showed complete hybridization with all of the amplicons indicating the repetitive nature of the sequence present downstream (Figure 9B). Sequencing of the 430 bp amplicon revealed an AT-rich sequence. Homology search identified the sequence to be homologous to the distal part of the *DCP2* UTR and the adjacent intergenic sequence between *DCP2* and *dbo*, the coordinates being 3L: 15826407..15826716. After aligning the

Table 6 Global overexpression of <italic>DCP2</italic> rescues the mutant phenotypes exhibited by <italic>l(3)tb</italic> homozygoytes

Genetic Crosses	*Act5C-GAL4/CyO; +/+* X *Act5C GAL4/CyO; +/+*		*+/+; Tub-GAL4/TM6B* X *+/+; Tub GAL4/TM6B*		*Act5C-GAL4/CyO; l(3)tb/TM6B* X *Sp/CyO; l(3)tb: UAS-DCP2/TM6B*		*UAS-DCP2/CyO; l(3)tb/TM6B* X *Sp/CyO; l(3)tb: Tub GAL4/ TM6B*	
	Homozygotes die as embryos or early larvae		Homozygotes die as embryos or early larvae		CyO and *TM6B* homozygotes die as embryos or early larvae		CyO and *TM6B* homozygotes die as embryos or early larvae	
01. Eggs	**750**		**790**		**1050**		**1245**	
02. Unfertilized Eggs	39	5.2%	37	4.7%	68	6.5%	86	6.9%
03. Fertilized Eggs	711	94.8%	753	95.3%	982	93.5%	1159	93.1%
04. Dead Embryos	304	42.8%	357	47.4%	434	44.2%	525	45.3%
05. Dead 1st and 2nd instar Larvae	8	1.12%	19	2.52%	34	3.46%	57	4.92%
06. Dead 3rd instar larvae	2	0.28%	5	0.66%	72	7.33%	128	11.04%
07. Pupae	**397**	55.8%	**372**	49.4%	**442**	45.0%	**449**	38.7%
08. Dead Pupae	17	4.3%	11	2.9%	21	4.8%	23	5.1%
09. Eclosion following over-expression of *DCP2* in homozygous *l(3)tb* background	—	—	—	—	*Act5C-GAL4/CyO; l(3)tb:UAS-DCP2/ l(3)tb*		*UAS-DCP2/CyO; l(3)tb: Tub-GAL4/ l(3)tb*	
					94	**21.3%**	77	**17.2%**
	—	—	—	—	*Act5C-GAL4/Sp; l(3)tb:UAS-DCP2 /l(3)tb*		*UAS-DCP2/Sp; l(3)tb: Tub-GAL4/ l(3)tb*	
					61	**13.8%**	89	**19.8%**

present set of reads with the previous set, a sequence duplication was observed for 5′-T-A-T-A-3′, flanking the *Gypsy*-LTR insertion (Supplementary Figure S6 B-3 and 4). The present set of sequencing reads also confirmed that the LTR insertion (3L: 15826407..15826407) was indeed prior to the completion of the UTR (3L: 15826423). Copy number variation analyses of the intergenic sequence *vs.* the internal control through PCR in the wild type and the mutant $DCP2^{l(3)tb,}$ showed a sharp increase in the amplicon concentration of the intergenic sequence in $DCP2^{l(3)tb}$ against the internal control as evidenced from the gel electrophoretogram (Figure 9C). Comparison of the fluorescent intensity of the bands (intra and inter-genotype) showed a relatively high ratio of concentrations of the amplicon to the internal control (*Dsor*) amplicon, as observed from the graphical analyses (Figure 9D). Based on the results obtained from rough and fine mapping, the architecture of the mutant allele, $DCP2^{l(3)tb}$ is depicted in Figure 9E, which shows the bipartite nature of the mutation, *viz*., amplification of the intergenic sequence between *DCP2* and *dbo*, as well as an insertion of 444 bp *Gypsy* LTR-like sequence immediately downstream to the TSS of *DCP2*.

$DCP2^{l(3)tb}$ is a DCP2 hypomorph along with low expression of the neighboring gene, dbo

Following the identification of the genomic architecture of the allele, it was imperative to determine the expression potential of the allele. Semi-quantitative RT-PCR analyses confirmed the hypomorphic nature of the allele wherein the homozygous *l(3)tb* mutant showed extremely low levels of expression of *DCP2* (Figure 9F). Since the intergenic region between *DCP2* and *dbo* is upstream to either gene and bears an expansion, *dbo* transcript titres were also examined wherein they showed extremely lowered expression (Figure 9F). At present, it is doubtful whether the lowered *dbo* level is a cause or an effect of the mutation since Dbo (Smac/Diablo/Henji) is a pro-apoptogenic molecule which inhibits the inhibitor of apoptotic proteins (IAP), and its lowered levels, therefore, serve as a prognostic marker of tumor progression in human carcinomas (Martinez-Ruiz *et al.*, 2008). Again, *dbo* expresses strongly in the neuronal tissues and localizes at the synapse (Wang *et al.*, 2016) where its perturbation causes alteration in neuromuscular function. Despite being a multi-faceted molecule, ubiquitous knock-down of *dbo* does not result in developmental abnormalities, *viz*., developmental delay, lethality or tumorous phenotypes in the brain, and/or wing imaginal discs (Supplementary Figure S7).

The tumor caused by DCP2 is hyperplastic with elevated Cyclin A and E

Since the mutation showed all the hallmarks of classical tumor suppressors (Merz *et al.*, 1990), we sought to characterize the perturbations in cellular physiology caused in the wake of tumourigenesis. RT-PCR analyses depicted elevated levels of Cyclin E (G1/S phase cyclin) and A (G2/M phase cyclin), which are indicative of increased cell proliferation and rapid cell cycles (Figure 10C). Immunolocalization studies also confirmed the elevated expression of Cyclin E as well (Figure 10A and B). On observing closely, the regular arrangement of cells in the brain hemisphere and optic lobes in the wild type was severely disrupted in the mutant along with excessive growth and increased number of mitotic nuclei. The enlarged brain lobes, increased number of mitotic nuclei and disruption of the regular arrangement of cells in the mutant concomitant with elevated expression of cyclins A and E validated the tumourous nature of the mutant.

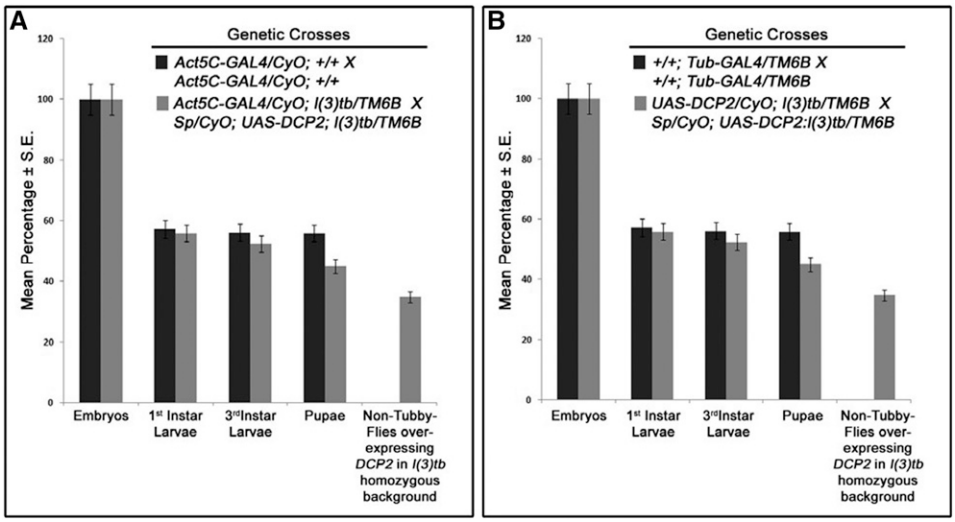

Figure 11 Global overexpression of *DCP2* rescues mutant phenotypes associated with *l(3)tb*. Global over-expression of *DCP2* using ubiquitous GAL4 drivers [*Act5C-GAL4* (A) or *Tub-GAL4* (B)] in the mutant homozygous *l(3)tb* individuals rescued the larval and pupal lethality. The graphs depict the fate of the non-tubby progeny, all of which pupated, devoid of any developmental anomalies and emerged as healthy flies.

When the tumorous brains (Figure 10D) and wing discs (Figure 10E) were examined for the expression of the polarity marker Discs large (Dlg), both tissues did not show appreciable loss of polarity. On a closer look, the wing discs at 138 h AEL showed an increase in cell number concomitant with a decrease in cell size (Figure 10E-C). At the same stage, the tumorous brain shows an increased number of cells in the optic lobe (Figure 10D). Usually, neoplastic tumors are metastatic and the tumor cells lose their polarity to acquire the mesenchymal-like fate, delaminate from the matrix and migrate. In contrast, hyperplastic tumors do not show appreciable loss of polarity even in later stages of tumourigenesis, since in these tumors the cells do not delaminate but remain adhered to the original tissue matrix, concomitant with cell division (Miles *et al.* 2011). The expression pattern of Dlg showed retention of polarity at 138 h of development, which is an exceptionally late and delayed 3rd instar larval stage, implying that tumor is an over-proliferative and hyperplastic. Again, this is in agreement with the Cyclin E staining pattern and taken together they imply excessive cell division, which essentially requires increased and rapid cell cycles.

Global overexpression of DCP2 rescues mutant phenotypes associated with l(3)tb

$DCP2^{l(3)tb}$ is essentially an insertion allele of *DCP2* and it was validated genetically by over-expressing *DCP2* using ubiquitous GAL4 drivers (*Act5C-GAL4* or *Tub-GAL4*) in the mutant homozygous *l(3)tb* individuals. Rescue in phenotype confirmed that $DCP2^{l(3)tb}$ to be an insertion allele of DCP2. Table 6 shows the genotype and fate of the progeny as scored from the rescue experiment. As can be seen, for over-expression of *DCP2* using *Act5C-GAL4*, out of 35.1% (N = 155) non-tubby progeny (*l(3)tb* homozygous background), *i.e.*, *Act5C-GAL4/CyO* or *Sp*; *l(3)tb:UAS-DCP2/l(3)tb*, 21.3% (N = 94) and 13.8% (N = 61) segregated as curly (*Act5C-GAL4/CyO*; *l(3)tb:UAS-DCP2/l(3)tb*) and non-curly (or with sternopleural bristles: *Act5C-GAL4/Sp*; *l(3)tb:UAS-DCP2/l(3)tb*), respectively. Similarly, while over-expressing using *Tub-GAL4*, we obtained 37% (N = 166) non-tubby progeny, *i.e.*, *UAS-DCP2/CyO* or *Sp*; *l(3)tb:Tub-GAL4/l(3)tb*, out of which, 17.2% (N = 77) were curly (*UAS-DCP2/CyO*; *l(3)tb:Tub-GAL4/l(3)tb*) while 19.8% (N = 89) were non-curly (*UAS-DCP2/ Sp*; *l(3)tb:Tub-GAL4/l(3)tb*) (Figure 11).

In both the cases of overexpression, all non-tubby progeny pupated, devoid of any developmental anomalies reminiscent of *l(3)tb* mutation, and emerged as flies. Thus, the rescue of the mutant phenotypes observed in *l(3)tb* homozygotes by global overexpression of *DCP2* iteratively substantiates the fact the *l(3)tb* is an allele of *DCP2* and that the tumor is caused solely owing to the loss of expression of *DCP2*.

Discussion and Conclusion

In the present paper we have identified a novel insertion allele of *Drosophila DCP2*, namely $DCP2^{l(3)tb,}$ through a mutagenesis screen. *DCP2* is conserved in other organisms and is extremely important for a number of growth processes throughout development (Xu *et al.*, 2006; Ma *et al.*, 2013), DNA replication (Mullen and Marzluff 2008; Schmidt *et al.*, 2011), stress response (Hilgers *et al.*, 2006; Xu and Chua 2012), synapse plasticity (Hillebrand *et al.*, 2010), retrotransposition (Dutko *et al.*, 2010) and viral replication (Hopkins *et al.*, 2013). In *Arabidopsis*, *DCP2* loss-of-function alleles show accumulation of capped mRNA intermediates, lethality of seedlings and defects in post-embryonic development, with no leaves, stunted roots with swollen root hairs, chlorotic cotyledons and swollen hypocotyls (Goeres *et al.*, 2007; Iwasaki *et al.*, 2007; Xu *et al.*, 2006). In humans as well, chromosomal deletions of 5q21-22, the region harboring *DCP2*, is frequently observed in lung cancers (Hosoe *et al.*, 1994; Mendes-da-Silva *et al.*, 2000), colorectal cancer (Delattre *et al.*, 1989) and oral squamous cell carcinoma (Mao *et al.*, 1998). Hence, *DCP2* has an unexplored role in the development and/or cell cycle progression across phyla, which needs to be investigated. Since the physiology of an organism is tightly regulated by the optimized titres of gene expression programs, a global loss of DCP2 may lead to perturbation in mRNA titres, which may alter the cellular response to such dismal conditions and eventually lead to drastic physiological disorders such as tumourigenesis. The exact mechanism(s) by which a loss of DCP2 leads to tumourigenesis needs further analysis and identification of the novel allele, $DCP2^{l(3)tb}$, unravels that *DCP2* could be a probable candidate for future explorations of tumourigenesis.

ACKNOWLEDGMENTS

The authors acknowledge Prof. L. S. Shashidhara, IISER Pune, India, Prof. Volker Hartenstein, University of California, USA for sharing the Anti-Armadillo and Anti-Deadpan antibodies, respectively and to Prof. Aike Guo, Institute of Biophysics, China for sharing *UAS-DCP2* fly line. We sincerely acknowledge Prof. Subhash C. Lakhotia, Prof.

Rajiva Raman and Dr. Rachana Nagar of our lab for assistance in fine mapping of the mutation and in analyses and interpretation of the results obtained therein. We duly acknowledge the National Facility for Laser Scanning Confocal Microscopy, UGC-CAS, DST-FIST of Department of Zoology, Banaras Hindu University and DST-PURSE, UGC-UPE to the Institute. We sincerely thank Department of Science and Technology (DST) for financial support to JKR.

LITERATURE CITED

Alone, D. P., 2002 Molecular genetic analysis of *Rab11 gene* in *Drosophila melanogaster*. PhD Thesis, Banaras Hindu University, India.

Banerjee, A., and J. K. Roy, 2018 Bantam regulates the axonal geometry of *Drosophila* larval brain by modulating actin regulator enabled. Invert. Neurosci. 18: 7. https://doi.org/10.1007/s10158-018-0212-8

Bier, E., H. Vaessin, S. Shepherd, K. Lee, K. McCall *et al.*, 1989 Searching for pattern and mutation in the *Drosophila* genome with a *P-lacZ* vector. Genes Dev. 3: 1273–1287. https://doi.org/10.1101/gad.3.9.1273

Coller, J., and R. Parker, 2004 Eukaryotic mRNA decapping. Annu. Rev. Biochem. 73: 861–890. https://doi.org/10.1146/annurev.biochem.73.011303.074032

Cooley, L., R. Kelley, and A. Spradling, 1988 Insertional mutagenesis of the *Drosophila* genome with single *P* element. Science 239: 1121–1128. https://doi.org/10.1126/science.2830671

Delattre, O., D. J. Law, Y. Remvikos, X. Sastre, A. P. Feinberg *et al.*, 1989 Multiple genetic alterations in distal and proximal colorectal cancer. Lancet 334: 353–356. https://doi.org/10.1016/S0140-6736(89)90537-0

Dunckley, T., and R. Parker, 1999 The DCP2 protein is required for mRNA decapping in *Saccharomyces cerevisiae* and contains a functional MutT motif. EMBO J. 18: 5411–5422. https://doi.org/10.1093/emboj/18.19.5411

Dutko, J. A., A. E. Kenny, E. R. Gamacheand, and M. J. Curcio, 2010 5′ to 3′ mRNA decay factors colocalize with Ty1 gag and human APOBEC3G and promote Ty1 retrotransposition. J. Virol. 84: 5052–5066. https://doi.org/10.1128/JVI.02477-09

Engeland, K., 2018 Cell cycle arrest through indirect transcriptional repression by p53: I have a DREAM. Cell Death Differ. 25: 114–132. https://doi.org/10.1038/cdd.2017.172

Gateff, E., and H. A. Schneiderman, 1969 Neoplasms in mutant and cultured wild-type tissues of *Drosophila*. Natl. Cancer Inst. Monogr. 31: 365–397.

Gateff, E., 1978 Malignant neoplasms of genetic origin in *Drosophila melanogaster*. Science 200: 1448–1459. https://doi.org/10.1126/science.96525

Gateff, E., 1994 Tumour suppressor and overgrowth suppressor genes of *Drosophila melanogaster*: developmental aspects. Int. J. Dev. Biol. 38: 565–590.

Gaviraghi, M., C. Vivori, Y. P. Sanchez, F. Invernizzi, A. Cattaneo *et al.*, 2018 Tumour suppressor PNRC1 blocks rRNA maturation by recruiting the decapping complex to the nucleolus. EMBO J. 37: e99179. https://doi.org/10.15252/embj.201899179

Goeres, D. C., J. M. Van Norman, W. Zhang, N. A. Fauver, M. L. Spencer *et al.*, 2007 Components of the *Arabidopsis* mRNA decapping complex are required for early seedling development. Plant Cell 19: 1549–1564. https://doi.org/10.1105/tpc.106.047621

Golic, K. G., and M. M. Golic, 1996 Engineering the *Drosophila* genome: chromosome rearrangements by design. Genetics 144: 1693–1711.

Hilgers, V., D. Teixeira, and R. Parker, 2006 Translation-independent inhibition of mRNA deadenylation during stress in *Saccharomyces cerevisiae*. RNA 12: 1835–1845. https://doi.org/10.1261/rna.241006

Hillebrand, J., K. Pan, A. Kokaram, S. Barbee, R. Parker *et al.*, 2010 The Me31B DEAD-box helicase localizes to postsynaptic foci and regulates expression of a CaMKII reporter mRNA in dendrites of *Drosophila* olfactory projection neurons. Front. Neural Circuits 4: 121. https://doi.org/10.3389/fncir.2010.00121

Hopkins, K. C., L. M. McLane, T. Maqbool, D. Panda, B. Gordesky-Gold *et al.*, 2013 A genome-wide RNAi screen reveals that mRNA decapping restricts bunyaviral replication by limiting the pools of Dcp2-accessible targets for cap-snatching. Genes Dev. 27: 1511–1525. https://doi.org/10.1101/gad.215384.113

Hosoe, S., K. Ueno, Y. Shigedo, I. Tachibana, T. Osaki *et al.*, 1994 A frequent deletion of chromosome 5q21 in advanced small cell and non-small cell carcinoma of the lung. Cancer Res. 54: 1787–1790.

Ivanov, A. I., C. Young, K. Den Beste, C. T. Capaldo, P. O. Humbert *et al.*, 2010 Tumour suppressor *scribble* regulates assembly of tight junctions in the intestinal epithelium. Am. J. Pathol. 176: 134–145. https://doi.org/10.2353/ajpath.2010.090220

Iwasaki, S., A. Takeda, H. Motose and Y. Watanabe, 2007 Characterization of *Arabidopsis* decapping proteins AtDCP1 and AtDCP2, which are essential for post-embryonic development. FEBS Let. 581: 2455–2459. https://doi.org/10.1016/j.febslet.2007.04.051

LaGrandeur, T. E., and R. Parker, 1998 Isolation and characterization of Dcp1p, the yeast mRNA decapping enzyme. EMBO J. 17: 1487–1496. https://doi.org/10.1093/emboj/17.5.1487

Lakhotia, S. C., and M. G. Tapadia, 1998 Genetic mapping of the amide response element(s) of *hsr-omega* locus of *Drosophila melanogaster*. Chromosoma 107: 127–135. https://doi.org/10.1007/s004120050288

Liebl, F. L., K. M. Werner, Q. Sheng, J. E. Karr, B. D. McCabe *et al.*, 2006 Genome-wide P-element screen for *Drosophila* synaptogenesis mutants. J. Neurobiol. 66: 332–347. https://doi.org/10.1002/neu.20229

Lindsley, D. L., and G. G. Zimm, 1992 *The genome of Drosophila melanogaster*, p. 1101, Acad. Press, Cambridge, MA.

Lukacsovich, T., Z. Asztalos, W. Awano, K. Baba, S. Kondo *et al.*, 2001 Dual-tagging gene trap of novel genes in *Drosophila melanogaster*. Genetics 157: 727–742.

Ma, J., M. Flemr, H. Strnad, P. Svoboda, and R. M. Schultz, 2013 Maternally recruited DCP1A and DCP2 contribute to messenger RNA degradation during oocyte maturation and genome activation in mouse. Biol. Reprod. 88: 11–21. https://doi.org/10.1095/biolreprod.112.105312

Mandal, L, 2001 Molecular genetic analysis of a new tumor suppressor gene, *l(3)tb*, and a small G-protein encoding gene, *Rab11*, in *Drosophila melanogaster*. PhD Thesis, Banaras Hindu University, India.

Mao, E. J., S. M. Schwartz, J. R. Daling and A. M. Beckmann, 1998 Loss of heterozygosity at 5q21–22 (*adenomatous polyposis coli* gene region) in oral squamous cell carcinoma is common and correlated with advanced disease. J. Oral Pathol. Med. 27: 297–302. https://doi.org/10.1111/j.1600-0714.1998.tb01960.x

Martinez-Ruiz, G., V. Maldonado, G. Ceballos-Cancino, J. P. R. Grajeda, and J. Melendez-Zajgla, 2008 Role of Smac/DIABLO in cancer progression. J. Exp. Clin. Cancer Res. 27: 48. https://doi.org/10.1186/1756-9966-27-48

Mechler, B. M., 1994 When the control is lacking—the role of tumour suppressor genes in cancer development. J. Biosci. 19: 537–556.

Mendes-da-Silva, P., A. Moreira, J. Duro-da-Cost, D. Matias, and C. Monteiro, 2000 Frequent loss of heterozygosity on chromosome 5 in non-small cell lung carcinoma. Mol. Pathol. 53: 184–187. https://doi.org/10.1136/mp.53.4.184

Merz, R., M. Schmidt, I. Török, U. Protin, G. Schuler *et al.*, 1990 Molecular action of the *l(2)gl* tumour suppressor gene of *Drosophila melanogaster*. Environ. Health Perspect. 88: 163–167. https://doi.org/10.1289/ehp.9088163

Miles, W. O., N. J. Dyson, and J. A. Walker, 2011 Modeling tumor invasion and metastasis in *Drosophila*. Dis Models Mech 4: 753–761.

Mitchell, P., and D. Tollervey, 2001 mRNA turnover. Curr. Opin. Cell Biol. 13: 320–325. https://doi.org/10.1016/S0955-0674(00)00214-3

Mugridge, J. S., and J. D. Gross, 2018 Decapping enzymes STOP "cancer" ribosomes in their tracks. EMBO J. 37: e100801. https://doi.org/10.15252/embj.2018100801

Mullen, T. E., and W. F. Marzluff, 2008 Degradation of histone mRNA requires oligouridylation followed by decapping and simultaneous degradation of the mRNA both 5′ to 3′ and 3′ to 5′. Genes Dev. 22: 50–65. https://doi.org/10.1101/gad.1622708

Novick, P., and M. Zerial, 1997 The diversity of Rab proteins in vesicle transport. Curr. Opin. Cell Biol. 9: 496–504. https://doi.org/10.1016/S0955-0674(97)80025-7

Papagiannouli, F., and B. M. Mechler, 2013 Modeling tumorigenesis in *Drosophila*: current advances and future perspectives. in: Future Aspects of Tumor Suppressor Genes. InTech publications pp. 97–128.

Parker, R., and H. Song, 2004 The enzymes and control of eukaryotic mRNA turnover. Nat. Struct. Mol. Biol. 11: 121–127. https://doi.org/10.1038/nsmb724

Raghavan, A., and P. R. Bohjanen, 2004 Microarray-based analyses of mRNA decay in the regulation of mammalian gene expression. Brief. Funct. Genomics 3: 112–124. https://doi.org/10.1093/bfgp/3.2.112

Ren, J., J. Sun, Y. Zhang, T. Liu, Q. Ren *et al.*, 2012 Down-regulation of Decapping Protein 2 mediates chronic nicotine exposure-induced locomotor hyperactivity in *Drosophila*. PLoS One 7: e52521. https://doi.org/10.1371/journal.pone.0052521

Russell, D. W., and J. Sambrook, 2001 Molecular cloning: a laboratory manual 1: 112. Cold Spring Harbor, NY.

Ryder, E., M. Ashburner, R. Bautista-Llacer, J. Drummond, J. Webster *et al.*, 2007 The DrosDel deletion collection: a *Drosophila* genome wide chromosomal deficiency resource. Genetics 177: 615–629.

Sambrook, J., E. F. Fritsch, and T. Maniatis, 1989 Molecular cloning: a laboratory manual. Cold Spring Harbor, NY.

Satoh, A. K., F. Tokunaga, and K. Ozaki, 1997 Rab proteins of *Drosophila melanogaster*: novel members of the Rab-protein family. FEBS Lett. 404: 65–69. https://doi.org/10.1016/S0014-5793(97)00094-X

Schmidt, M. J., S. West, and C. J. Norbury, 2011 The human cytoplasmic RNA terminal U-transferase ZCCHC11 targets histone mRNAs for degradation. RNA 17: 39–44. https://doi.org/10.1261/rna.2252511

She, M., C. J. Decker, D. I. Svergun, A. Round, N. Chen *et al.*, 2008 Structural basis of dcp2 recognition and activation by dcp1. Mol. Cell 29: 337–349. https://doi.org/10.1016/j.molcel.2008.01.002

Song, M. G., Y. Li, and M. Kiledjian, 2010 Multiple mRNA decapping enzymes in mammalian cells. Mol. Cell 40: 423–432. https://doi.org/10.1016/j.molcel.2010.10.010

Thibault, S. T., M. A. Singer, W. Y. Miyazaki, B. Milash, N. A. Dompe *et al.*, 2004 A complementary transposon tool kit for *Drosophila melanogaster* using P and piggyBac. Nat. Genet. 36: 283–287. https://doi.org/10.1038/ng1314

Tipping, M., and N. Perrimon, 2014 *Drosophila* as a model for context-dependent tumorigenesis. J. Cell. Physiol. 229: 27–33.

Wang, M., P. Y. Chen, C. H. Wang, T. T. Lai, P. I. Tsai *et al.*, 2016 Dbo/Henji modulates synaptic dPAK to gate glutamate receptor abundance and postsynaptic response. PLoS Genet. 12: e1006362. https://doi.org/10.1371/journal.pgen.1006362

Wang, Z., X. Jiao, A. Carr-Schmid, and M. Kiledjian, 2002 The hDcp2 protein is a mammalian mRNA decapping enzyme. Proc. Natl. Acad. Sci. USA 99: 12663–12668. https://doi.org/10.1073/pnas.192445599

Watson, P.M., S. W. Miller, M. Fraig, D. J. Cole, D. K. Watsonand, *et al.*, 2008 CaSm (LSm-1) overexpression in lung cancer and mesothelioma is required for transformed phenotypes. Am. J. Resp. Cell Mol. 38: 671–678. https://doi.org/10.1165/rcmb.2007-0205OC

Xu, J., J. Y. Yang, Q. W. Niu, and N. H. Chua, 2006 *Arabidopsis* DCP2, DCP1, and VARICOSE form a decapping complex required for postembryonic development. The Plant Cell. 18: 3386–3398.

Xu, J., and N. H. Chua, 2012 Dehydration stress activates *Arabidopsis* MPK6 to signal DCP1 phosphorylation. EMBO J. 31: 1975–1984. https://doi.org/10.1038/emboj.2012.56

Communicating editor: E. Gavis